Integrating data from chevron traps and video cameras into a standardized index of abundance for vermilion snapper, *Rhomboplites aurorubens*

Daniel C. Gwinn, Nathan M. Bacheler, and Kyle Shertzer

SEDAR55-WP07

Submitted: 8 December 2017

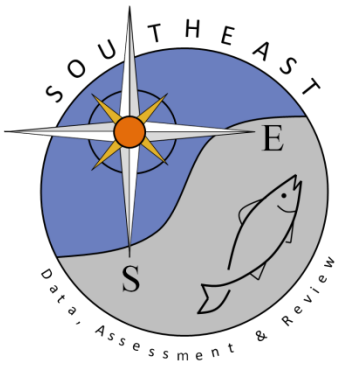

Please cite this document as:

Gwinn, D. C., N. M. Bacheler, and K. Shertzer. Integrated data from chevron traps and video cameras into a standardized index of abundance for vermilion snapper (*Rhomboplites aurorubens*). SEDAR55-WP07. SEDAR, North Charleston, SC. 59 pp.

SEDAR55-WP07

Integrating data from chevron traps and video cameras into a standardized index of abundance for vermilion snapper (*Rhomboplites aurorubens*)

[1]Daniel C. Gwinn, [2]Nathan M. Bacheler and [2]Kyle Shertzer

[1] Biometric Research, South Fremantle, Western Australia, Australia.
[2] National Marine Fisheries Service, Southeast Fisheries Science Center, Beaufort, North Carolina, United States of America.

Abstract

Standardized chevron trap sampling has been used since 1990 to monitor reef fish along the southeast Atlantic coast. Since 2011, video cameras have been paired with chevron traps creating two semi-independent fisheries indices. Here we develop a State-Space Model for vermilion snapper to combine both chevron trap catches and video counts into a single integrated abundance index for stock assessment. The index spans the time frame of 1990-2016 and accounts for variation in sampling efficiency of both sampling gears as well as covariates describing the spatial distribution of fish. The index is meant to describe population trends of vermilion snapper in the region. Index values for 2015-2016 include a calibration factor to account for a change in camera type.

Table of Contents

Background

Many economically important reef fish species along the southeast US Atlantic coast have been monitored using fishery-independent chevron fish traps since 1990. Since 2011, cameras have been attached to chevron traps to provide an additional index of reef fish abundance. Early research comparing trap catches to video counts showed substantial variation between the two (Bacheler et al. 2013a), likely due to differences in how environmental conditions influenced the ability of traps and videos to detect various species of fish (Bacheler et al. 2014, Coggins et al. 2014). For instance, vermilion snapper and gray triggerfish were more likely observed in traps than by video when water temperature was warm, and more likely observed by video when water was clear (Bacheler et al. 2014). At a 2015 stock assessment workshop for red snapper and gray triggerfish (SEDAR 41), chevron trap and video data were used to compute separate indices of abundance that were subsequently combined following the method of Conn (2010). Workshop attendees noted that the gears lacked independence since cameras were attached to traps, but attendees also were unwilling to discard one of the indices because no other fishery-independent indices were available and because both gear types were considered informative. The method we propose here combines trap and video data into a single time series so information from both is used while accounting for the lack of independence between the two gears.

One methodological approach to combine trap and video data is through the use of hierarchical model structures that can separate aspects of the ecological process of interest from aspects of the observation process (Gelman et al. 2007, Royle and Dorazio 2008). There are few effective ways to achieve this separation with count-based data, but two examples include *N*-mixture models (Royle 2004) and State-Space Models (SSM, Schnute 1994). The application of *N*-mixture models to fish is fairly new in the fisheries literature and quite rare (but see Webster et al. 2008, Flowers and Hightower 2013, Chambert et al. 2016, Scheerer et al. 2017). The paucity of examples of *N*-mixture models applied to fish is likely a result of the stringent assumptions required by these models. Because *N*-mixture models rely on the variance of replicate count data to separate the abundance from the detection process, strict population closure and a binomial sampling process are required for useful model performance (Barker et al. 2017). Indeed, preliminary analysis of vermilion snapper data indicated random extra-binomial variation in the replicate camera counts and dependence of the camera counts on the chevron trap due to its depleting effects on the local abundance during the first ~100 min of sampling. These types of extra-binomial variation and dependencies make the application of *N*-mixture models impractical.

Alternatively, State-Space Models have a long history in fisheries (e.g. Schnute 1994, Maunder et al. 2013, Shertzer et al. 2016) and have been applied to integrate multiple data types into a single index (e.g. Conn 2010, Staton et al. 2017). Because SSMs do not rely on binomial sampling to estimate "true" abundance and detection probability, they require fewer assumptions. SSMs typically are applied to time series data and assume that catch (trap catch or camera counts) is a random variable drawn from a specified distribution with a mean that is equal to the true relative abundance each year. For the parameters of this model to be estimable, the assumption also is made that the true relative abundance is non-independent among years, which is a biologically valid assumption for most biota with multi-year lifespans.

Here we develop a novel fishery-independent index of abundance for vermilion snapper in the US South Atlantic through the development and application of a State-Space Model using trap and video data collected by the Marine Resources Monitoring, Assessment, and Prediction (MARMAP) program (1990-2016), the Southeast Area Monitoring and Assessment Program South Atlantic (SEAMAP-SA, 2009-2016), and the Southeast Fishery-Independent Survey (2010-2016). Collectively, these three fishery-independent sampling programs are referred to as the Southeast Reef Fish Survey (SERFS). The SSM has three key features that make it particularly useful for this application: (i) The model incorporates the chevron trap catches and camera counts into a single index and has the potential to incorporate additional information as available. (ii) The model corrects for shifts in the sampling frame by modeling temporal variation at the meta-population level separate from spatial variation at the sub-population level. (iii) The model corrects for changes in sampling efficiency due to temporal and spatial variation in the environment through the use of covariates of detection and random effects.

Data and Treatment

There were 15,629 chevron trap samples available covering a period of 27 years (1990-2016). For the time period of 2011-2016, the chevron traps were fitted with a video camera resulting in 7,644 41-frame video samples available. For analysis, we used un-transformed catch of the chevron trap and the sum of the counts across the 41 camera frames (*SumCount*). We chose to use the *SumCount* of the camera data because (i) preliminary analysis indicated that modeling each of 41 camera frames for each video sample substantially increase computation time, (ii) *SumCount* changes linearly with the mean count (Bacheler and Carmichael 2014), which is often the preferred camera metric (Conn 2011, Schobernd et al. 2014), and (iii) using the *SumCount* preserves the discrete nature of the camera counts allowing for the use of derivations of the Poisson distribution to describe both the chevron trap and camera observation processes.

We applied several data filters to simplify predictor variables, remove records with missing predictor variables, or remove unusual values. We removed any data points in which the survey video was considered unreadable by an analyst (e.g., too dark, corrupt video file), or if the trapping event was flagged for any irregularity that could have affected catch rates (e.g., trap dragged or bounced). Additionally, any survey video for which fewer than 41 video frames were read (n =150) was removed from the full data set. Standardizing the number or readable frames for any data point was essential due to our use of *SumCount* as a response variable. We also identified any chevron trap or video sample in which corresponding predictor variables were missing and removed them from the final data set. After the filtering process, the final data set contained 13,903 chevron trap samples, of which 6,767 had corresponding video camera samples (Table 1). R code used to filter the data is provided in Appendix A.

The Model

We fit the chevron trap catch and video *SumCount* data to a State-Space Model (SSM) that described patterns in vermilion snapper relative abundance through space and time. Our SSM was formulated in a hierarchical framework with a sub-model that described patterns in

"true" relative abundance and two secondary sub-models that described the observation of the "true" relative abundance with chevron traps and video cameras. By modeling the abundance process and observation process with separate sub-models we were able to separate observation error from process error and account for some aspects of systematic variation in sampling efficiency (i.e. detection probability).

Our model describes changes in the standardized relative abundance (hereafter referred to simply as abundance, N_t) from year to year with an exponential growth model as:

$$\log(N_t) = \log(N_{t-1}) + r_t \quad (1)$$

where r_t represents the log-scale change in abundance between time *t*-1 and time *t*. Abundance was treated as an unobserved (latent) variable and represents the time series of primary interest (i.e., the standardized index). The parameter r_t was modeled as a random variable on the log scale drawn from a normal distribution as:

$$r_t \sim \text{Normal}(\bar{r}, \sigma) \quad (2)$$

where $\bar{r}$ is the expected population change between time *t*-1 and *t*, and σ is the standard deviation, representing the magnitude of process error.

Spatial variation in abundance across sample sites each year was modeled as:

$$n_{s,t} = \log(N_t) + cov_{s,t}^{n} + \varepsilon^{abun} \quad (3)$$

where the term $\log(N_t)$ is the year specific intercept of the linear model, $cov_{s,t}^{n}$ is a linear combination of spatial covariates, and ε^{abun} describes random spatial variation in abundance that is unexplained by the covariate structure.

We approximated the chevron trap catches ($c_{s,t}^{trap}$) and the camera *SumCounts* ($c_{s,t}^{cam}$) as deviates drawn from Poisson log-Normal distributions, which are similar in character to negative binomial distributions (Nitzoufras 2009, p. 315-317), but can demonstrate better mixing properties than negative binomial distributions when applied in Bayesian programs such as JAGS. We specified these models as:

$$c_{s,t}^{trap} \sim \text{Poisson}\left(e^{n_{s,t} + cov_{t,j}^{trap} + \varepsilon^{trap}}\right) \quad (4)$$

$$c_{s,t}^{cam} \sim \text{Poisson}\left(e^{n_{s,t} + cov_{t,j}^{cam} + \varepsilon^{cam} + \nu_t}\right) \quad (5)$$

where the mean on the log scale is the site-specific abundance $n_{s,t}$ plus a linear combination of environmental and sampling covariates (i.e. $cov_{t,j}^{trap}$ and $cov_{t,j}^{cam}$) to account for systematic variation in sampling efficiency. The parameters ε^{trap} and ε^{cam} are gear-specific log-Normal distributed random observation errors modeled as, $\varepsilon_{s,t} \sim Normal(0, \sigma)$, with a mean of zero and an estimated standard deviation specific to each sampling method (i.e.

σ^{trap} and σ^{cam}). The parameter ν_t is a fixed value (i.e. log(1.72)) that accounts for the increased field of view of the video cameras used in 2015 and 2016.

Model Covariates

We incorporated a suite of covariates into our abundance and observation models. We selected covariates based on two key considerations. Our first consideration was to separate covariates that influenced the spatial distribution of fish from those that influenced temporal patterns in fish abundance. This was important because spatial and temporal patterns of abundance are modeled in two separate hierarchical layers (i.e. equation 1 and 3) to create a distinction between the fishery index, i.e. temporal patters in abundance at the meta-population level (N_t), from spatial variation in the data due to patterns in the spatial distribution of fish and shifts in the sampling frame through time ($n_{s,t}$). Thus, we include a main and quadradic effect of latitude (*lat* and lat^2), longitude (*lon* and lon^2) and depth (*depth* and $depth^2$), as well as the potential interaction between latitude and longitude as covariates of local-scale abundance. We included both main and quadratic effects of these variables to account for any optimal ranges in latitude, longitude and depth within our sampling frame that vermilion snapper may prefer. The interaction between latitude and longitude was included to allow any preferred range of one variable to be dependent on the other. For example, if vermilion snapper demonstrated a preferred distance from shore, a positive interaction between latitude and longitude could approximate this spatial distribution. Spatial covariates of abundance were incorporated into the model as:

$$cov_{s,t}^{n} = \beta_1 lat_{s,t} + \beta_2 lat_{s,t}^2 + \beta_3 depth_{s,t} + \beta_4 depth_{s,t}^2 + \beta_5 lon_{s,t} + \beta_6 lon_{s,t}^2 + \beta_7 lat_{s,t} lon_{s,t}. \quad (6)$$

Our second key consideration was to separate covariates of the abundance and detection processes. This was important because our model likely has limited ability to disentangle systematic patterns in abundance from systematic patterns in detection when they are similar. Thus, we do not expect to be able to resolve the effects of covariates that have similar influences on patterns in abundance as they do on patterns in detection (Barker et al. 2017). Under this consideration, the most useful covariates for predictive purposes are those that either, (i) only influence the abundance or the detection process, or (ii) have very different influences on the abundance and detection processes. Thus, we included main and quadratic effects of trap soak time (*E* and E^2), main and quadratic effects of temperature (*temp* and $temp^2$), water turbidity (*turb*), percent hardbottom substrate (*sub*), bottom relief (*relf*), current direction (*dir1* and *dir2*), and attached biota (*bio*) into our chevron trap observation model.

Another consideration was that certain covariates were measured using the camera (i.e. *turb*, *sub*, *relf*, *dir1*, *dir2*, and *bio*) and were, thus, only available for the time period of 2011-2016, while other covariates (i.e. *E*, E^2, *temp*, and $temp^2$) were available for the entire time period of our data set. This was not an issue for the camera detection sub-model, but it required us to model chevron trap detection covariates separately for the time period of 1990-

2010 and 2011-2016. We, therefore, incorporated covariates of chevron trap detection for the time period of 1990-2010 into the model as:

$$cov_{s,t}^{trap} = \eta_1 E_{s,t} + \eta_2 E_{s,t}^2 + \eta_3 temp_{s,t} + \eta_4 temp_{s,t}^2 \quad (7)$$

and for the time period of 2011-2016 as:

$$cov_{s,t}^{trap} = \eta_1 E_{s,t} + \eta_2 E_{s,t}^2 + \eta_3 temp_{s,t} + \eta_4 temp_{s,t}^2 + \eta_5 turb_{s,t} + \eta_6 sub_{s,t} + \eta_7 relf_{s,t} + \eta_8 dir1_{s,t} + \eta_9 dir2_{s,t} + \eta_{10} bio_{s,t} \quad (8)$$

where the subscript *t* represents samples collected between 1990 and 2010 for equation 7 and between 2011 and 2016 for equation 8.

In the camera detection sub-model, we included turbidity, current direction, main and quadratic effects of bottom temperature, percent hardbottom substrate and attached biota as:

$$cov_{s,t}^{cam} = \varphi_1 + \varphi_2 turb_{s,t} + \varphi_3 dir1_{s,t} + \varphi_4 dir2_{s,t} + \varphi_5 temp_{s,t} + \varphi_6 temp_{s,t}^2 + \varphi_7 sub_{s,t} + \varphi_8 relf_{s,t} + \varphi_9 bio_{s,t} \quad (9)$$

where φ_1 allows for a systematic difference in the detection probability of the camera relative to the chevron trap. All covariate definitions are provided in Table 2.

Model Fit Test

We evaluated model fit for eight general model error structures with Bayesian p-values (*Bp*, Kery 2010). The Bayesian p-value is a posterior predictive check that provides a measure of under- or over-dispersion of the data relative to the model (Kery 2010, Hooten and Hobbs 2015, Broms et al. 2016). The eight model error structures included models that either included or excluded the random variables ε^{abun}, ε^{trap}, and/or ε^{cam}. Because these parameters are random effects, they offer little predictive advantage when included in our models, however, evaluating how their inclusion or exclusion impacts general model fit is necessary to accurately describe the magnitude and shape of the residual error, to partition the residual error between biological and observation processes and to appropriately estimate the uncertainty in our model parameters and predictions (Kery and Schaub 2012).

To perform the model fit evaluation, we first randomly selected 100 data points from each of six data categories to validate the fit of our models. Our categories were, (i) trap catches = zero prior to 2011, (ii) trap catches = zero post 2010, (iii) trap catches > zero prior to 2011, (iv) trap catches > zero post 2010, (v) camera *SumCounts* = zero, and (vi) camera *SumCounts* > zero. We expected that understanding how our model fit each of these data types would provide comprehensive insight into the model's ability to back predict our fishery index. For each selected data point, we simulated the corresponding trap or video count for each Markov Chain Monte Carlo (MCMC) iteration and calculated a Pearson residual between the simulated and expected value (i.e. predicted χ^2) and observed and expected value (i.e. observed χ^2). The simulated data are considered "perfect" because they are generated directly from the model and, thus, the resultant Pearson residual represents the

fit of the model when all model assumptions are perfectly met (Kery 2010). We then created a fit metric that is equal to zero when the Pearson residual was greater for the observed data than the simulated data and is equal to one, otherwise. The *Bp* was then calculated as the mean of the posterior sample of the fit metric for each taxon, where a mean of 0.5 indicates perfect model fit to the data and a mean approaching 1 or 0 indicates under- or over-dispersion of the data relative to the model, respectively. We further investigated model fit with diagnostic plots of site-specific Bayesian p-values for non-zero data and residual plots (Appendix C-J). However, because count data drawn from derivations of a Poisson distribution with small expected values do not conform to a Chi-square distribution (Pierce and Schafer 1986) we also calculated the site-specific probability of predicting a zero for count data with observed values equal to zero (Appendix C-J).

Variable Selection for Index Prediction

For the fishery index prediction, we used the best fitting model (determined with the model fit test) that included only the subset of covariate effects that were statistically different from zero (i.e. statistically significant) for each sub-model. However, if a main effect was not statistically different from zero, but a quadratic effect or interaction with the variable was, we included the main effect in the model. We evaluated the statistical significance of all covariates by summarizing the posterior distributions of the best model determined by our model fit test. We considered covariates statistically significant if their 95% Bayesian credible intervals did not overlap with zero. This approach to determining statistically significant variables approximates an $\alpha = 0.05$ and is a common approach taken in Bayesian statistics when the risk of overparameterization is low (which is likely the case for this data set given a total of 13,903 sample locations used to fit the model; e.g. Burton et al. 2012, Beesley et al. 2015, King et al. 2016).

Model Fitting Methods

The posterior distributions of all parameters were estimated using a Gibbs sampler implemented in JAGS (Plummer 2003). We called JAGS from program R (R Core Team 2015) using the library R2jags (Su and Yajima 2015). All prior distributions of log-scale covariate effect parameters were specified as diffuse normal distributions. Standard deviation parameters were specified as Gamma distributions with shape parameters equal to 0.01 and were verified to not influence the range of posterior distributions. Inference was drawn from 10,000 posterior samples taken from two chains of 500,000 samples. We discarded the first 250,000 values of each chain to remove the effects of initial values and thinned the chain to every 50th value. Convergence of all models was diagnosed by visual inspection of trace plots and Gelman-Rubin statistic ($\hat{R} \leq 1.1$ indicate model convergence, Gelman et al. 2004). JAGS model code is provided in Appendix B.

Results and Discussion

All models converged after 500,000 iterations and required up to 74 hours of computer processing of two MCMC chains run in parallel. Our posterior-predictive check indicated that three of our models adequately fit our data (models 1, 2, & 3 in Table 3). All of these models included a random effect in the abundance sub-model (ε^{abun}) and either a

random effect in the camera sub-model (ε^{cam}), the trap sub-model (ε^{trap}), or both. Further inspection of residual plots provided little evidence of additional support for any one of the three models (Appendices C, D, and E) indicating that our models could not fully disentangle the variability in the data due to process noise in the spatial distribution of abundance and noise due to unexplained variation in sampling efficiency. However, estimated temporal patterns in the indices of abundance were nearly identical among these three models indicating that results are robust to this uncertainty in the optimal model error structure (See Figures C4, D4, and E4 in Appendix C, D, and E). Alternatively, there were subtle differences in the covariate effect estimates among the three top model error structures that could alter the conclusion about the statistical significance of six covariates including *depth*, *lon* (abundance sub-model), *relief*, *dir1*, *dir2* (trap sub-model), and *turb* (camera sub-model). The difference in the covariate effect estimates and their standard errors tended to be small, but never-the-less resulted in changes in credible interval overlap with zero (see Appendix K). For this working paper we chose to allow the model the opportunity to partition the variability among sub-models by using? the full model with all random effects (model 1 in Table 3, Log-N Poisson$^{\text{abun \& cam \& trap}}$) to produce the index of abundance and evaluate covariate effects.

Our covariate evaluation procedures indicated that most of our covariates had a statistically significant influence on abundance or detection (Table 4). This result is not surprising since we selected covariates based on our *a priori* expectation that they may influence these processes. The direction of the covariate effects on the observation sub-models tended to be consistent with previous research on the sampling efficiency of these gears. For example, we found a dome-shaped effect of soak time on the chevron trap sampling efficiency where the maximum efficiency equates to a soak time of approximately 110 min with reductions in sampling efficiency for soak times of shorter or longer intervals (Figure 2). This relationship of chevron trap efficiency and soak time has been observed for multiple fish species, including vermillion snapper (Bacheler et al. 2013b, Bacheler et al. 2013c). Similarly, we found that the sampling efficiency of both sampling gears tended to be invariant to temperature when the bottom temperature was low, but sharply increased at temperatures greater than 24°C (Figure 2 and 3). This result corroborates the findings of Bacheler et al. (2014) for vermillion snapper. Alternatively, we observed a positive effect of percent hard-bottom substrate on the sampling efficiency of both gears (Figures 2 and 3). This result is in contrast to the negative effect of percent hard-bottom substrate on the sampling efficiency of chevron traps observed by Bacheler et al. (2014). However, the relative positive effect of hard-bottom substrate on camera sampling efficiency is much greater than for the chevron traps (φ_7 vs η_6, Table 4), which may give the appearance of a negative effect for chevron traps when unaccounted for in the camera observation model.

Three covariate effect estimates were not statistically different from zero. These included the main effect of depth in the abundance sub-model (β_3 , Table 4), the effect of water turbidity in the chevron trap sub-model (η_5, Table 4), and the effect of bottom relief in the chevron trap sub-model (η_7, Table 4). Because the quadratic effect of depth was statistically significant in the abundance sub-model (β_4, Table 4), we retained the main effect for the fishery index prediction. However, we removed the covariate effect of water turbidity

and bottom relief in the chevron trap sub-model for index prediction. The model excluding η_5 and η_7 demonstrated a lower value of DIC (Spiegelhalter et al. 2002) than the fully parameterized model (model 1 in Table 3). The DIC for the fully parameterized model 1 was 42063.8, whereas the DIC of model 1 excluding η_5 and η_7 was 41371.7, suggesting increased out-of-sample predictive performance for the reduced version. The annual index of abundance predicted by the reduced version of model 1 is presented in Table 5 and Figure 4. The index demonstrates a statistically significant negative linear trend through time (Figure 5).

One of the expected benefits of our SSM is that it accounts for shifts in the sampling frame from year to year. For example, over the length of time of the Southeast Reef Fish Survey sampling program, the number of chevron traps set each year has systematically increased as the program expanded (particularly since 2011). The expanding of this program has led to changes in the distribution of traps relative to latitude, longitude, and depth. Panel (a) of Figure 6 shows the average latitude, longitude, and depth of traps set for each year of the program (values are scaled for plotting). There is variability in the mean covariate values among years with apparent systematic increases in depth and decreases in latitude over the life of the program. Panel (b) of Figure 6 demonstrates the predicted observed change in abundance at the meta-population level when these covariates are not accounted for. Although the uncertainty in the metric is high, we can see a systematic bias in observed abundance that increases over time, which is fully accounted for in our final SSM models.

References

Bacheler, N.M., and Carmichael, J.T. 2014. Southeast reef fish survey video index development workshop. Final Report, National Marine Fisheries Service and South Atlantic Fisheries Management Council.

Bacheler, N.M., Schobernd, C.M., Schobernd, Z.H., Mitchell, W.A., Berrane, D.J., Kellison, G.T., and Reichert, M.J.M. 2013a. Comparison of trap and underwater video gears for indexing reef fish presence and abundance in the southeast United States. Fisheries Research, 143: 81-88.

Bacheler, N.M., Bartolino, V., and Reichert, M.J.M. 2013b. Influence of soak time and fish accumulation on catches of reef fishes in a multispecies trap survey. Fishery Bulletin, 111: 218-232.

Bacheler, N.M., Schobernd Z.H., Berrane, D.J., Schobernd, C.M., Mitchell, W.A., and Geraldi, N.R. 2013c. When a trap is not a trap: converging entry and exit rates and their effect on trap saturation of black sea bass (*Centropristis striata*). ICES Journal of Marine Science, 70: 873-882.

Bacheler, N.M., Berrane, D.J., Mitchell, W.A., Schobernd, C.M., Schobernd, Z.H., Teer, B.Z., Ballenger, J.C. 2014. Environmental conditions and habitat characteristics influence trap and video detection probabilities for reef fish species. Marine Ecology Progress Series, 517: 1-14.

Barker, R. J., Schofield, M. R., Link, W. A., and Sauer, J. R. 2017. On the reliability of N-mixture models for count data. Biometrica, doi:10.1111/biom.12734

Beesley, L.S., Gwinn, D.C., Price, A., King, A.J., Gawne, B., Koehn, J.D., Nielsen, D.L. 2014. Juvenile fish response to wetland inundation: how antecedent conditions can

inform environmental flow policies for native fish. Journal of Applied Ecology, 51: 1613-1621.

Broms, K. M., Hooten, M. B., and Fitzpatrick, R. M. 2016. Model selection and assessment for multi-species occupancy models. Ecology, 97: 1759-1770.

Burton, A.C., Sam, M.K., Balangtaa, C., and Brashares, J.S. 2012. Hierarchical multi-species modelling of carnivore responses to hunting, habitat and prey in a West African protected area. PLoS One, 7, e38007.doi:10.1371/journal.pone.0038007.

Carlin, B. R., and Chib, S. 1995. Bayesian model choice via Markov Chain Monte Carlo methods. Journal of the Royal Statistical Society B, 57: 473–484.

Chambert, T., Hossack, B.R., Fishback, L., and Davenport, J.M. 2016. Estimating abundance in the presence of species uncertainty. Methods in Ecology and Evolution, 7: 1041-1049.

Coggins, L.G, Bacheler, N.M., and Gwinn, D.C. 2014. Occupancy models for monitoring marine fish: a Bayesian hierarchical approach to model imperfect detection with a novel gear combination. PLoS ONE 9, e108302. doi:10.1371/journal.pone.0108301.

Conn, P.B. 2010. Hierarchical analysis of multiple noisy abundance indices. Canadian Journal of Fisheries and Aquatic Sciences, 67: 108–120.

Conn, P. B. 2011. An Evaluation and Power Analysis of Fishery Independent Reef Fish Sampling in the Gulf of Mexico and U. S. South Atlantic. NOAA Tech. Memorandum NMFS-SEFSC-610.

Flowers, H.J., and Hightower, J.E. 2015. Estimating sturgeon abundance in the Carolinas using side-scan sonar. Marine and Coastal Fisheries: Dynamics, Management, and Ecosystem Science, 7: 1-9.

Hooten, M. B., and Hobbs, N. T. 2015. A guide to Bayesian model selection for ecologists. Ecological Monographs, 85: 3-28.

Kéry, M., and Schaub, M. 2012. Bayesian population analysis using WinBUGS: A hierarchical perspective. Academic Press.

King, A. J., Gwinn, D. C., Tonkin, Z., Mahoney, J., Raymond, S., and Beesley, L. 2016. Using abiotic drivers of fish spawning to inform environmental flow management. Journal of Applied Ecology, 53: 34-43.

Maunder, M.N., Deriso, R.B., and Hanson, C.H. 2015. Use of state-space population dynamics models in hypothesis testing: advantages over simple log-linear regressions for modeling survival, illustrated with application to longfin smelt (*Spirinchus thaleichthys*). Fisheries Research, 164: 102-111.

Ntzoufras, I. 2009. Bayesian modeling using WinBUGS. Wiley.

Pierce, D.A., and Schafer, D.W. 1986. Residuals in Generalized Linear Models. Journal of the American Statistical Association, 81: 977–986.

Plummer, M. 2003. "JAGS: a program for analysis of Bayesian graphical models using Gibbs sampling." In *Proceedings of the 3rd International Workshop on Distributed Statistical computing (DSC 2003). March*, pp. 20-22.

R Core Team. 2015. R: A language and environment for statistical computing. R Foundation for Statistical Computing, Vienna, Austria. URL http://www.R-project.org/.

Royle, J.A. 2004. N-mixture models for estimating population size from spatially replicated counts. Biometrics, 60: 108-115.

Royle, J.A., and Dorazio, R.M. 2008. Hierarchical modeling and inference in ecology: the analysis of data from populations, metapopulations and communities. Academic Press, Waltham.

Scheerer, P.C., Peterson, J.T., and Clements, S. 2017. Distribution and abundance of millicoma dace in the Coos River basin, Oregon. Northwestern Naturalist, 98: 39-47.

Schnute, J.T. 1994. A general framework for developing sequential fisheries models. Canadian Journal of Fisheries and Aquatic Science, 51: 1676-1488.

Schobernd, Z.H., Bacheler, N.M., and Conn, P.B. 2014. Examining the utility of alternative video monitoring metrics for indexing reef fish abundance. Canadian Journal of Fisheries and Aquatic Science, 71: 464-471.

Shertzer, K.W., Bacheler, N.M., Coggins, L.G., Fieberg, J. 2016. Relating trap capture to abundance: a hierarchical state-space model applied to black sea bass (*Centropristis striata*) ICES Journal of Marine Science, 73: 512–519.

Spiegelhalter, D. J., Best, N.G., Carlin, B. P., and van der Linde, A. 2002. Bayesian measures of model complexity and fit. Journal of the Royal Statistical Society B, 64: 583–639.

Staton, B.A., Catalano, M.J., and Fleischman, S.J. 2017. From sequential to integrated Bayesian analyses: exploring the continuum with a Pacific salmon spawner-recruit model. Fisheries Research, 186: 237-247.

Yu-Sung Su and Masanao Yajima, (2015). R2jags: Using R to Run 'JAGS'. R package version 0.5-6. http://CRAN.R-project.org/package=R2jags.

Webster, R.A., Pollock, K.H., Ghosh, S.K., and Hankin, D.G. 2008. Bayesian spatial modeling of data from unit-count surveys of fish in streams. Transactions of the American Fisheries Society, 137: 438-453.

White, A.M., Zipkin, E.F., Manley, P.N., and Schlesinger, M.D. 2013. Conservation of avian diversity in the Sierra Nevada: moving beyond a single-species management focus. PLoSONE 8:e63088.

Tables

Table 1. Summary of data and the spatial attributes of the sample frame each year.

Year	# of video samples	# of trap samples	Depth Range (m)	Latitude range (ºN)	Longitude range (ºW)
1990	0	313	17 - 93	30.42 - 33.82	80.62 - 77.28
1991	0	272	17 - 95	30.75 - 34.61	80.62 - 76.17
1992	0	288	17 - 62	30.42 - 34.32	80.33 - 76.81
1993	0	392	16 - 94	30.44 - 34.32	80.90 - 76.81
1994	0	390	16 - 93	30.74 - 33.82	80.90 - 77.26
1995	0	382	16 - 60	29.78 - 33.75	80.90 - 77.28
1996	0	361	14 - 100	27.92 - 34.33	80.37 - 76.81
1997	0	401	15 - 97	27.87 - 34.59	80.90 - 76.64
1998	0	425	14 - 92	27.44 - 34.59	80.90 - 76.10
1999	0	215	15 - 75	27.27 - 34.41	80.89 - 76.71
2000	0	299	15 - 101	28.95 - 34.28	80.89 - 76.49
2001	0	252	14 - 91	27.87 - 34.28	80.90 - 76.40
2002	0	244	13 - 94	27.86 - 33.95	80.90 - 76.75
2003	0	224	16 - 92	27.43 - 34.33	80.54 - 76.81
2004	0	282	14 - 91	29.00 - 33.97	80.90 - 76.51
2005	0	303	15 - 69	27.33 - 34.32	80.48 - 76.39
2006	0	297	15 - 94	27.27 - 34.39	80.37 - 76.57
2007	0	337	15 - 92	27.33 - 34.33	80.89 - 76.51
2008	0	303	15 - 92	27.27 - 34.59	80.48 - 76.81
2009	0	404	14 - 91	27.27 - 34.60	80.90 - 76.39
2010	0	752	14 - 92	27.34 - 34.59	80.90 - 76.39
2011	542	542	15 - 93	27.23 - 34.54	81.22 - 76.40
2012	1009	1009	15 - 106	27.23 - 35.02	81.22 - 75.45
2013	1106	1106	15 - 100	27.33 - 35.01	81.22 - 75.45
2014	1358	1358	15 - 110	27.23 - 35.01	81.22 - 75.45
2015	1350	1350	16 - 110	27.26 - 35.02	81.22 - 75.45
2016	1402	1402	17 - 115	27.23 - 35.01	81.22 - 75.45

Table 2. Covariate descriptions and definitions.

Variable	Abbreviation	Class	Definition
Latitude	*lat*	continuous	The latitude of the sample location.
Longitude	*lon*	continuous	The longitude of the sample location.
Depth	*depth*	continuous	A continuous variable indicating the water depth at the trap location.
Soak time	*E*	continuous	A continuous variable indicating the length of time the trap was set before retrieval.
Temperature	*temp*	continuous	The water bottom temperature at the trap locations during sampling.
Turbidity	*turb*	categorical	A dummy variable indicating the level of turbidity (1 = level 2, 0 = level 1).
Substrate	*sub*	continuous	The proportion of visible substrate that is hard bottom.
Relief	*relf*	categorical	A dummy variable with value of 1 indicating that the relief was “high”.
Current away	*dir1*	categorical	A dummy variable that is 1 when the current direction is flowing away from the camera lens.
Current side	*dir2*	categorical	A dummy variable that is 1 when the current direction is flowing from the side of the camera lens.
Biota	*bio*	continuous	The percent cover of attached biota visible during any video.

Table 3. Bayesian p-values for model fit evaluation. The superscript "z" indicates observations that are equal to zero and the superscript "n" indicates non-zero observations. A value of 0.5 indicates perfect model fit, and values approaching 1 or 0 indicate under- or over-dispersion, respectively.

#	Model	2011 - 2016				1990 - 2010	
		Camera^{z}	Trap^{z}	Camera^{n}	Trap^{n}	Trap^{z}	Trap^{n}
1	Log-N Poisson$^{abun\ \&\ cam\ \&\ trap}$	0.38	0.68	0.51	0.48	0.65	0.50
2	Log-N Poisson$^{abun\ \&\ trap}$	0.56	0.17	0.47	0.57	0.50	0.54
3	Log-N Poisson$^{abun\ \&cam}$	0.38	0.68	0.51	0.48	0.66	0.50
4	Log-N Poisson$^{cam\ \&\ trap}$	0.99	1.00	0.36	0.53	1.00	0.54
5	Log-N Poisson^{abun}	0.00	0.00	0.00	0.00	0.60	0.47
6	Log-N Poisson^{trap}	0.00	1.00	0.00	0.53	1.00	0.56
7	Log-N Poisson^{cam}	0.56	0.00	0.51	0.00	0.00	0.00
8	Poison	0.00	0.00	0.00	0.00	0.00	0.00

Table 4. Covariate parameter posterior summaries. Posterior means, standard deviations and credible intervals are derived from posterior samples of the full model (model 1 in Table 3). The parameter flag indicates when the 95% credible intervals of posterior samples excludes zero (1=yes, 0=no).

Variable	Parameter	Mean	Standard deviation	95% Credible intervals	Parameter flag
Abundance					
Latitude	β_1	-1.47	0.35	-2.20, -0.80	1
Latitude^2	β_2	-1.05	0.13	-1.31, -0.79	1
Depth	β_3	0.10	0.08	-0.07, 0.26	0
Depth^2	β_4	-0.14	0.02	-0.19, -0.10	1
Longitude	β_5	0.90	0.30	0.33, 1.52	1
Longitude^2	β_6	-1.05	0.15	-1.36, -0.77	1
Lat:Lon	β_7	0.79	0.27	0.27, 1.31	1
Trap detection					
Soak time	η_1	3.93	0.82	2.32, 5.58	1
Soak time^2	η_2	-2.36	0.61	-3.56, -1.16	1
Temperature	η_3	0.82	0.05	0.72, 0.92	1
Temperature^2	η_4	0.10	0.01	0.08, 0.13	1
Turbidity	η_5	0.06	0.12	-0.19, 0.30	0
Substrate	η_6	0.66	0.10	0.46, 0.86	1
Relief	η_7	-0.43	0.22	-0.85, 0.02	0
Current away	η_8	0.65	0.17	0.34, 0.99	1
Current side	η_9	0.30	0.14	0.01, 0.59	1
Biota	η_{10}	-0.30	0.10	-0.49, -0.11	1
Camera detection					
Turbidity	φ_2	0.79	0.15	0.49, 1.08	1
Current away	φ_3	1.08	0.20	0.70, 1.45	1
Current side	φ_4	0.45	0.18	0.09, 0.82	1
Temperature	φ_5	0.37	0.08	0.21, 0.52	1
Temperature^2	φ_6	0.06	0.03	0.01, 0.10	1
Substrate	φ_7	1.27	0.12	1.02, 1.50	1
Relief	φ_8	0.91	0.22	0.44, 1.34	1
Biota	φ_9	-0.30	0.12	-0.52, -0.06	1

Table 5. Posterior summaries of the index of abundance (i.e. the predicted annual relative abundance of the meta-population).

Year	N_t	Scaled index	SD	2.5% CI	97.5% CI	CV
1990	0.0571	0.8150	0.0234	0.0244	0.1161	0.4097
1991	0.3054	4.3584	0.1152	0.1411	0.5855	0.3772
1992	0.1480	2.1116	0.0566	0.0657	0.2825	0.3824
1993	0.1073	1.5309	0.0410	0.0483	0.2079	0.3822
1994	0.2157	3.0779	0.0783	0.0999	0.4072	0.3630
1995	0.0892	1.2723	0.0325	0.0416	0.1657	0.3645
1996	0.0883	1.2600	0.0342	0.0393	0.1723	0.3877
1997	0.0436	0.6228	0.0175	0.0194	0.0850	0.4004
1998	0.0533	0.7603	0.0200	0.0244	0.1007	0.3749
1999	0.0850	1.2128	0.0345	0.0362	0.1679	0.4055
2000	0.0903	1.2890	0.0335	0.0403	0.1697	0.3712
2001	0.0859	1.2256	0.0343	0.0373	0.1706	0.3997
2002	0.1046	1.4928	0.0406	0.0474	0.2049	0.3884
2003	0.0289	0.4117	0.0132	0.0113	0.0620	0.4583
2004	0.0365	0.5215	0.0149	0.0154	0.0722	0.4068
2005	0.0333	0.4758	0.0136	0.0146	0.0668	0.4066
2006	0.0242	0.3460	0.0100	0.0103	0.0495	0.4136
2007	0.0392	0.5593	0.0156	0.0172	0.0779	0.3979
2008	0.0522	0.7453	0.0198	0.0232	0.1002	0.3792
2009	0.0530	0.7557	0.0200	0.0236	0.1002	0.3784
2010	0.0418	0.5963	0.0146	0.0202	0.0767	0.3501
2011	0.0160	0.2280	0.0062	0.0072	0.0308	0.3888
2012	0.0198	0.2822	0.0071	0.0094	0.0369	0.3576
2013	0.0102	0.1463	0.0038	0.0048	0.0196	0.3745
2014	0.0139	0.1987	0.0048	0.0068	0.0256	0.3412
2015	0.0166	0.2367	0.0056	0.0084	0.0300	0.3395
2016	0.0327	0.4671	0.0117	0.0154	0.0614	0.3582

Figures

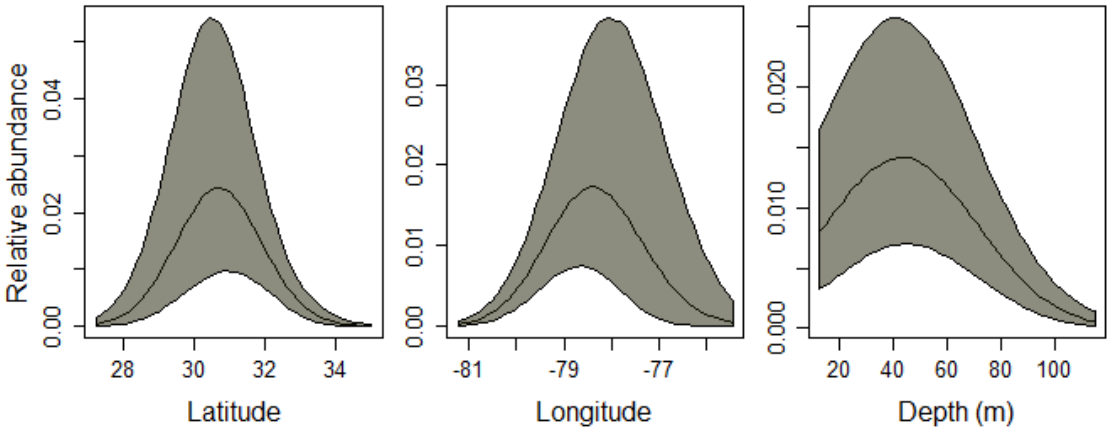

Figure 1. The predicted response of sub-population abundance to spatial covariates. The gray region represents 95% Bayesian credible intervals.

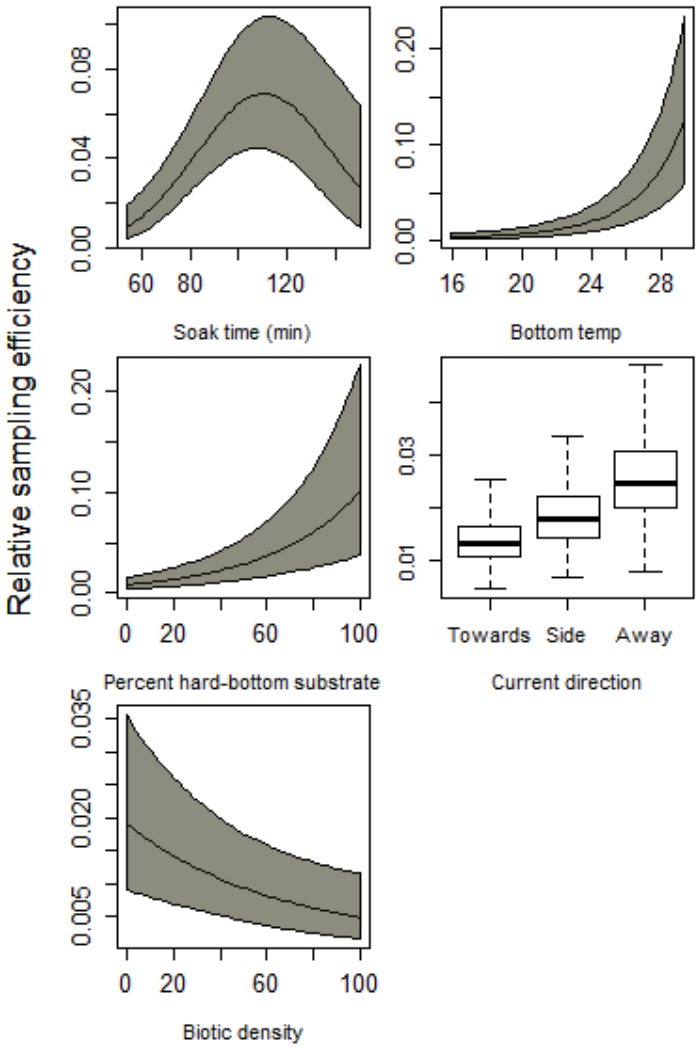

Figure 2. The predicted response of chevron trap sampling efficiency to sampling and environmental covariates. The gray region represents 95% Bayesian credible intervals.

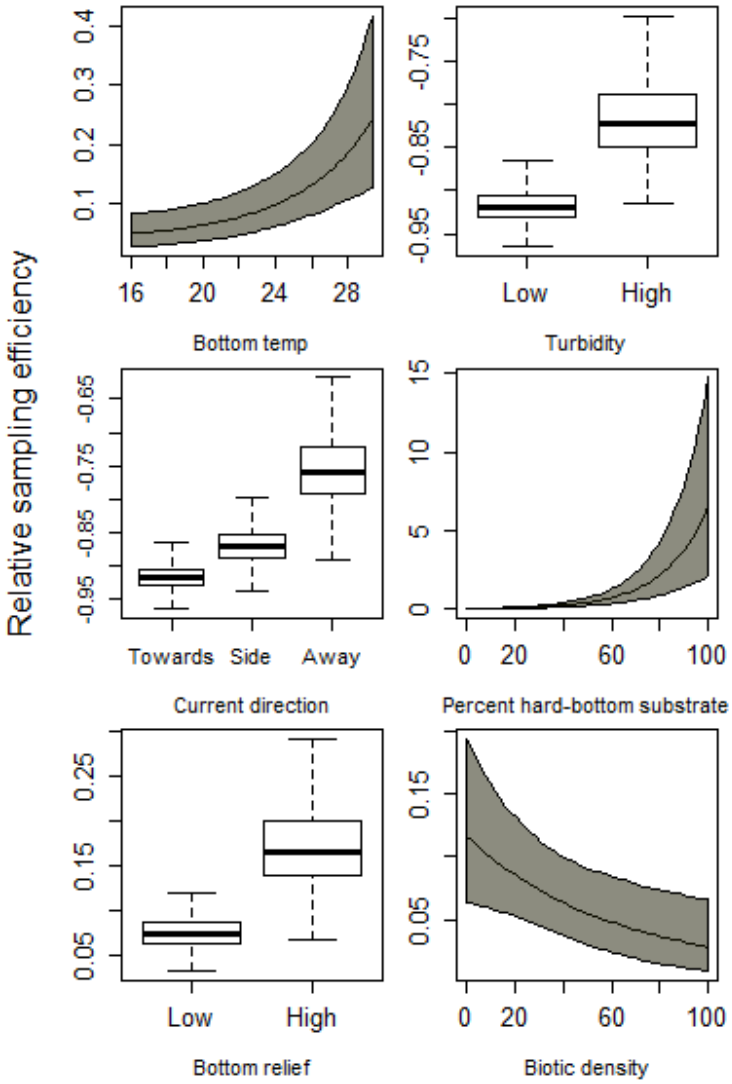

Figure 3. The predicted response of video camera sampling efficiency to sampling and environmental covariates. The gray region represents 95% Bayesian credible intervals.

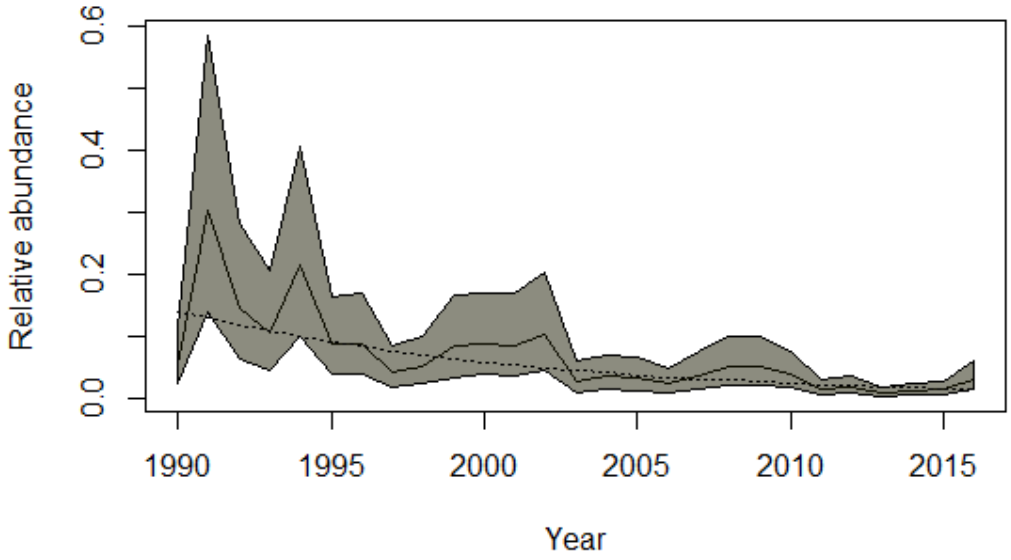

Figure 4. The predicted annual relative abundance of the vermilion snapper meta-population. The gray region represents 95% Bayesian credible intervals. The dotted line represents the estimated linear trend.

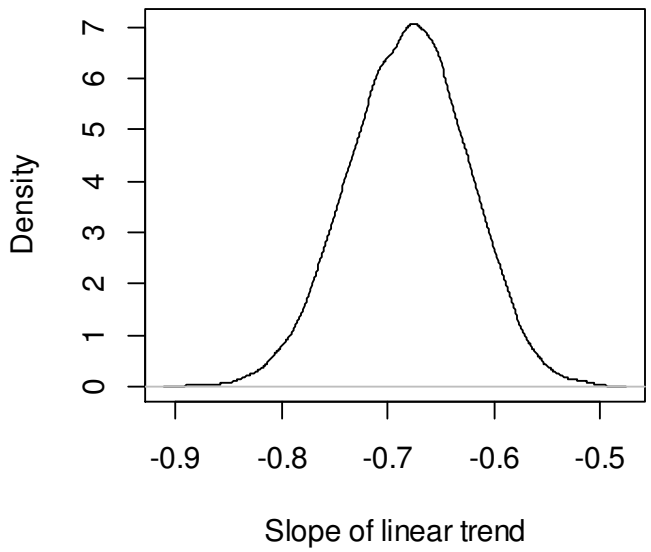

Figure 5. The posterior distribution of the slope of the linear trend in annual abundance between 1990 and 2016.

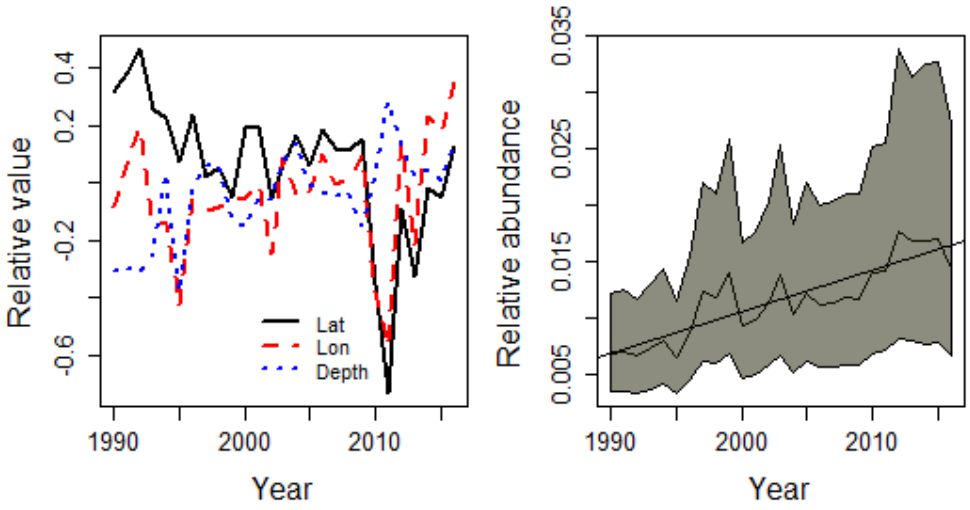

Figure 6. Impact of changing sampling frame on the predicted relative abundance at the meta-population level. The gray region represents 95% Bayesian credible intervals.

Appendix A. R code for filtering data

```
#-------------------------------------------------------------------------------#
#  FILTER DATA
#-------------------------------------------------------------------------------#
#Data records where both trap and camera were employed
 subrecords = which((dat_tmp$year>=2011) &
 !is.na(dat_tmp$temp) &
 !is.na(dat_tmp$depth)&
 !is.na(dat_tmp$lat) &
 (dat_tmp$current_direction!='unknown') &
(dat_tmp$no.readable.frames==41)&
 (dat_tmp$current_direction!='') &
(dat_tmp$turbidity!='unknown') &
(dat_tmp$turbidity!=2)&
 !is.na(dat_tmp$biotic_density) &
(dat_tmp$soaktime<=150) &
(dat_tmp$soaktime>=50)&
 !is.na(dat_tmp$percent_substrate) &
(dat_tmp$depth<=150) &
(dat_tmp$percent_substrate!='Unknown')&
 (dat_tmp$percent_substrate!='unknown') &
(dat_tmp$biotic_density!='unknown'))
#Data records when only the trap was employed
 brecords = which((dat_tmp$year<2011) &
!is.na(dat_tmp$temp) &
!is.na(dat_tmp$depth)&
 !is.na(dat_tmp$lat) &
(dat_tmp$soaktime<=150) &
(dat_tmp$soaktime>=50) &
(dat_tmp$depth<=150))
```

Appendix B. State-Space Model JAGS code

```
model {
#PREDICTIONS FOR MODEL FIT
#MODEL FOR TIME PERIOD 2011-2016
 #CAMERA OBSERVATION MODEL
  for(i in 1:cn){
  cc[i] ~ dpois(cam_exp[i])
  cam_exp[i] <- exp(cam_exp_b[i]+epic[i])
  cam_exp_b[i] <- (N[i]+log_pc[i]+camcorr[i])
  epic[i] <-0#~ dnorm(0,tau[2]) T(-10,10)
 #TRAP OBSERVATION MODEL
  tc[i] ~ dpois(trp_exp[i])
  trp_exp[i]  <- exp(trp_exp_b[i]+epit[i])
  trp_exp_b[i]  <- (N[i]+log_pt[i]+log_ptc[i])
  epit[i] ~ dnorm(0,tau[1]) T(-10,10)
 #ABUNDANCE MODEL
  N[i] <- lam_cov[i] + Npred[year[i]] + epin[i]
  epin[i] ~ dnorm(0,tau[4]) T(-10,10)
   }
#MODEL FOR TIME PERIOD 1990-2010
  for(i in (cn+1):n){
 #TRAP OBSERVATION MODEL
  tc[i] ~ dpois(trp_exp[i])
  trp_exp[i]<- exp(trp_exp_b[i]+epit[i])
  trp_exp_b[i]<- (N[i]+log_pt[i])
  epit[i] ~ dnorm(0,tau[1]) T(-10,10)
 #ABUNDANCE MODEL
  N[i] <- lam_cov[i] + Npred[year[i]] + epin[i]
  epin[i] ~ dnorm(0,tau[4]) T(-10,10)
   }
#COVARIATE VECTORS
 #Abundance covariates
   lam_cov[1:n] <- bet[1]*lat[] + bet[2]*lat2[] + bet[3]*depth[] +
                   bet[4]*depth2[] + bet[5]*lon[] + bet[6]*lon2[] +
                   bet[7]*lat[]*lon[]
 #Trap detection covariates
   log_pt[1:n] <- eta[1]*effort[] + eta[2]*effort2[] + eta[3]*temp[] +
                  eta[4]*temp2[]
   log_ptc[1:cn] <- eta[5]*turb[] + eta[6]*substrate[] + eta[7]*relief[] +
                    eta[8]*dir1[] + eta[9]*dir2[] + eta[10]*biota[]
 #Camera detection covariates
   log_pc[1:cn] <- phi[1] + phi[2]*turb[] + phi[3]*dir1[] + phi[4]*dir2[] +
                   phi[5]*ctemp[] + phi[6]*ctemp2[] + phi[7]*substrate[] +
```

```
                phi[8]*relief[] + phi[9]*biota[]

#TEMPORAL ABUNDANCE PROCESS MODEL (exponential population growth w/ AR1
process error)
  for(i in 2:nyr){
  Npred[i] <- Npred[i-1] + r[i]
  r[i] ~ dnorm(rmu,tau[3])
  }
  Npred[1] ~ dnorm(0,.1)
  r[1] ~ dnorm(rmu[1],tau[3])
  rmu ~ dnorm(0,.1)
#PRIOR DISTRIBUTIONS
  for(i in 1:7){bet[i] ~ dnorm(0,0.1)}
  for(i in 1:10){eta[i] ~ dnorm(0,0.1)}
  for(i in 1:9){ phi[i] ~ dnorm(0,0.1)}
  for(i in 1:5){
  tau[i] <- pow(sig[i],-2)
  sig[i] ~ dt(0,1/(0.3^2),2) T(0,10)
  }
}
```

Appendix C. Model fit diagnostic plots (Log-N Poisson$^{abun\ \&\ cam\ \&\ trap}$).

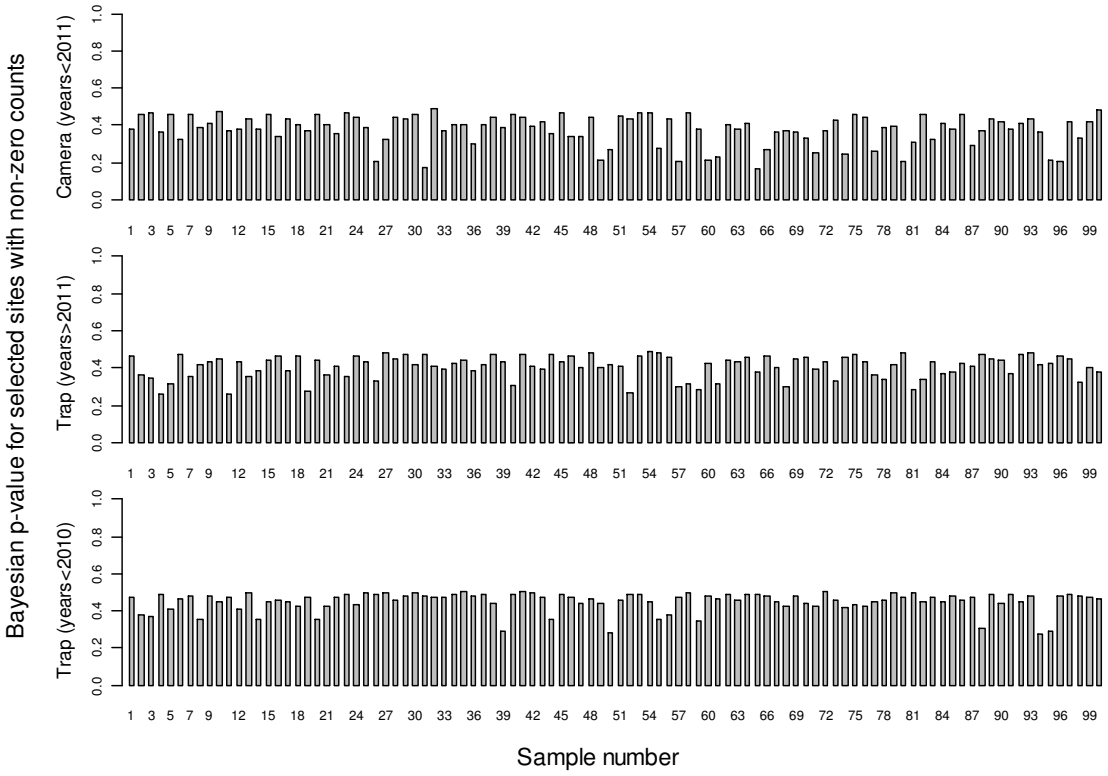

Figure C1. The Bayesian p-values for model-fit references sites with non-zero counts.

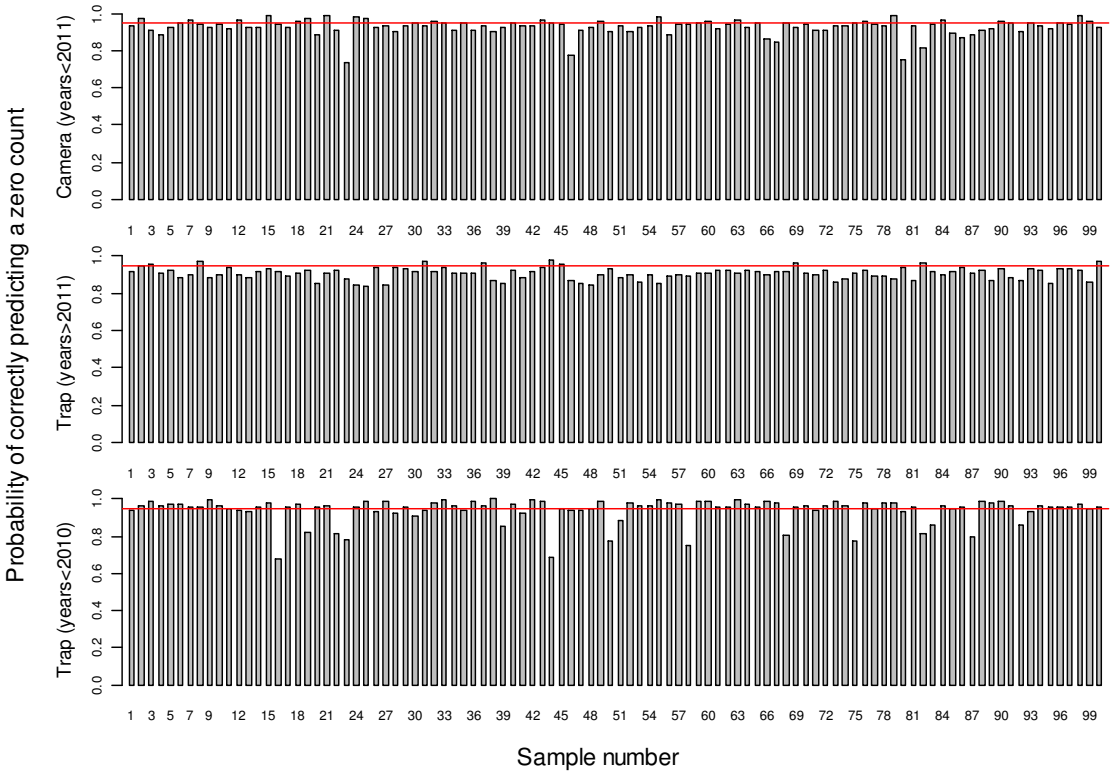

Figure C2. The model probability of correctly predicting a count equal to zero when the true count is zero. The horizontal red line represents a probability of 0.95.

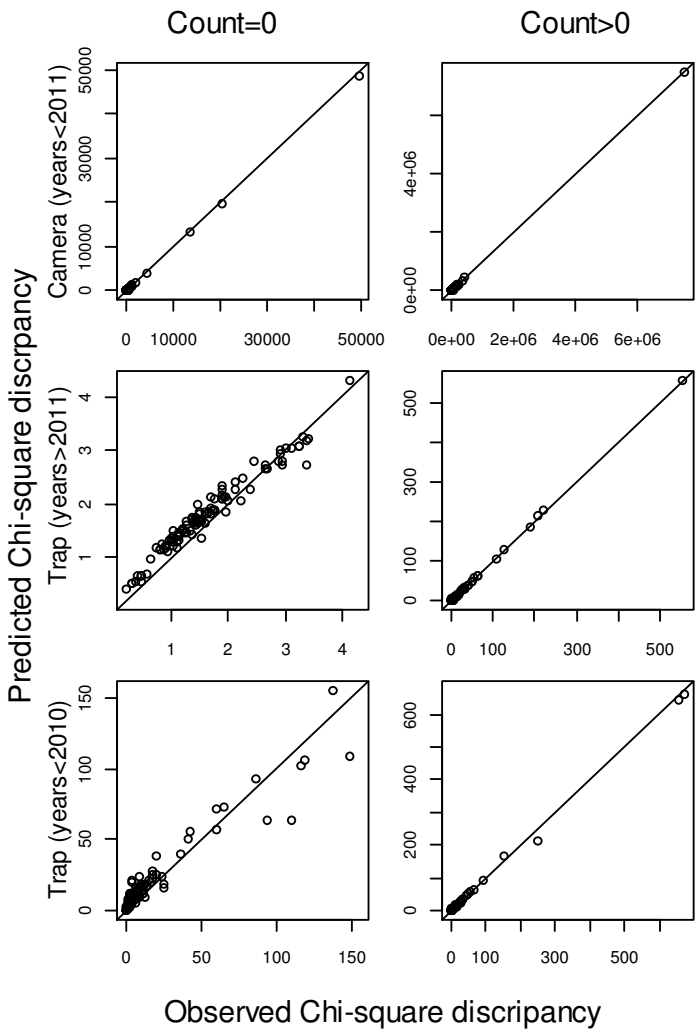

Figure C3. Residual plots of the observed and predicted Pearson residual for each model-fit reference site. The left column represents count data that are equal to zero, while the right column represents count data that are greater than zero.

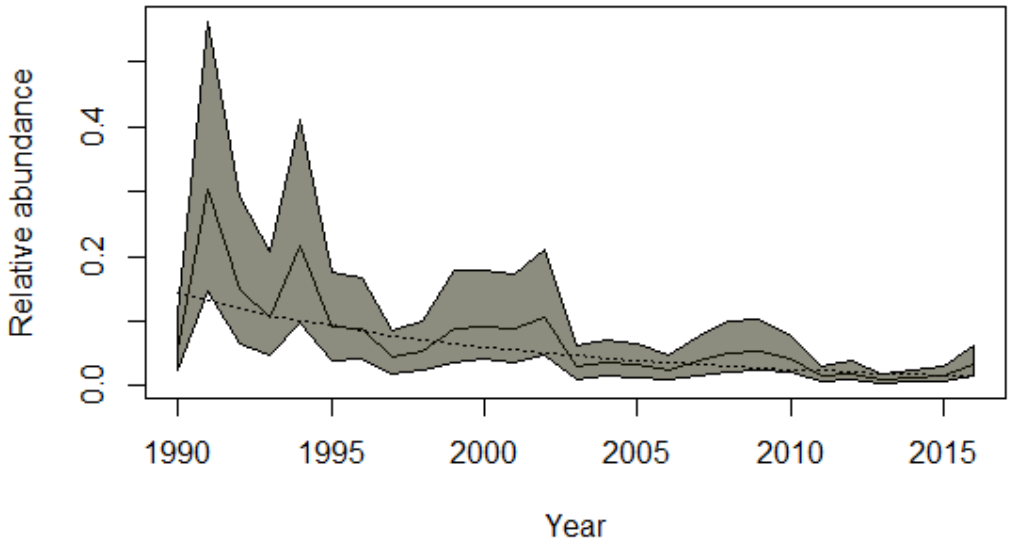

Figure C4. The predicted annual relative abundance of the vermilion snapper meta-population. The gray region represents 95% Bayesian credible intervals. The dotted line represents the estimated linear trend.

Appendix D. Model fit diagnostic plots (Log-N Poisson$^{abun\ \&\ trap}$).

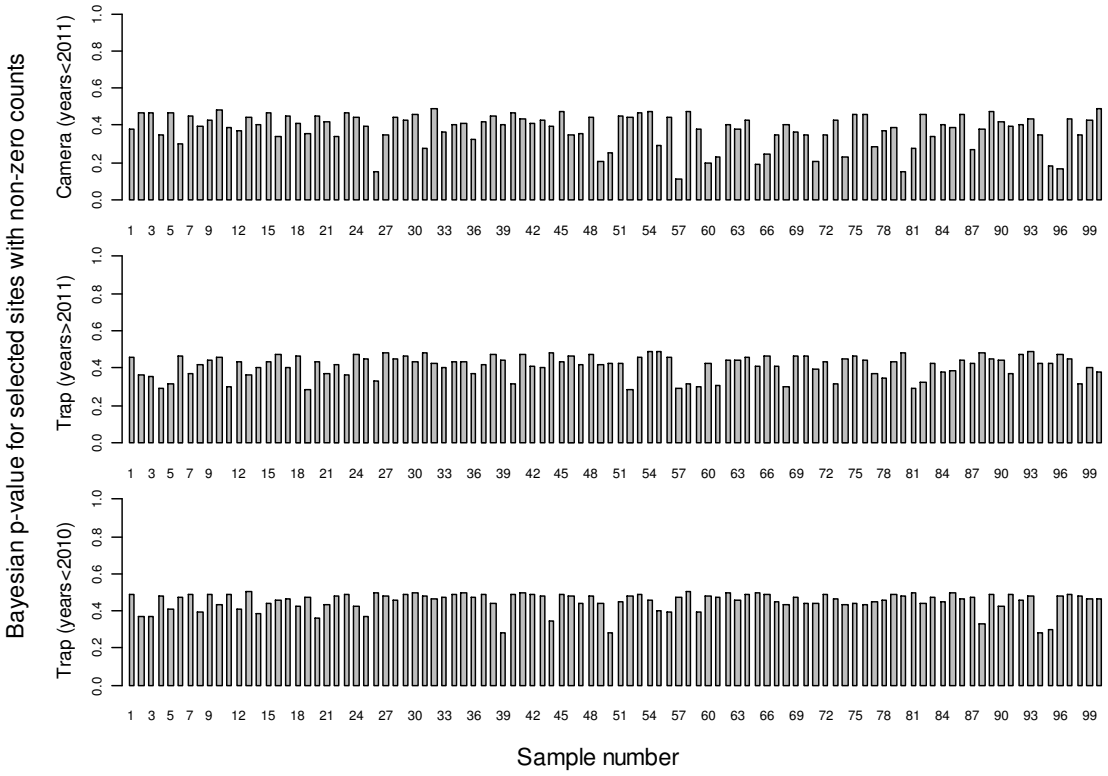

Figure D1. The Bayesian p-values for model-fit references sites with non-zero counts.

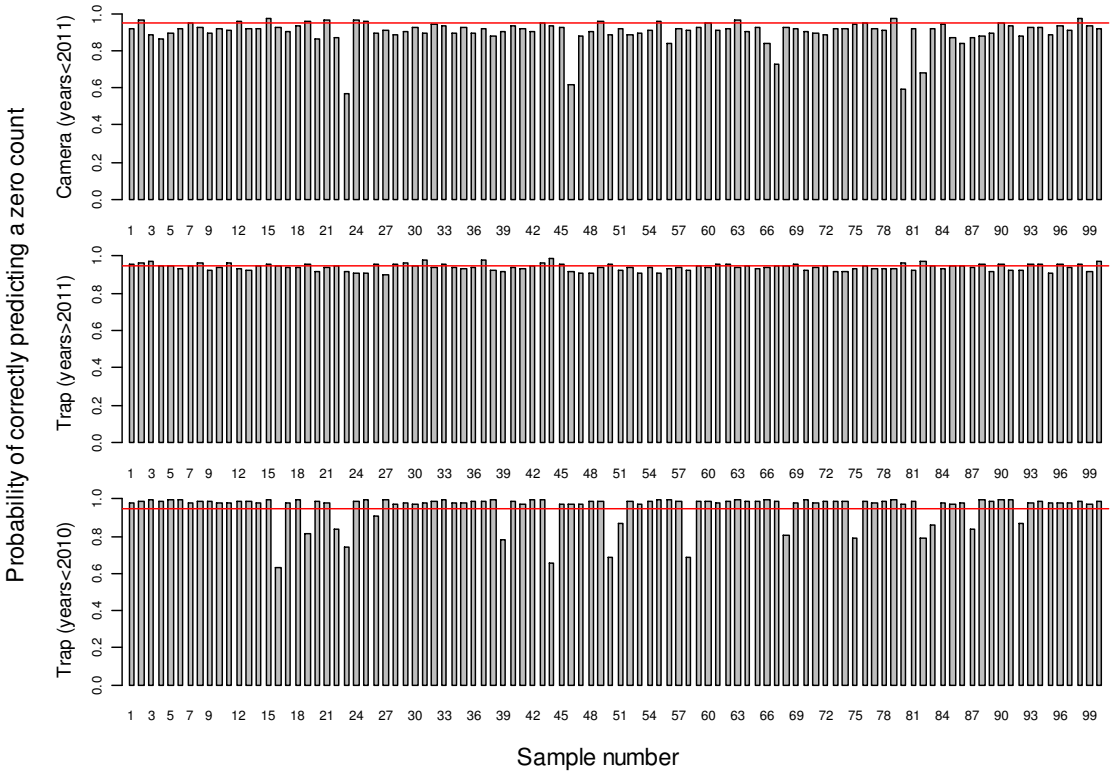

Figure D2. The model probability of correctly predicting a count equal to zero when the true count is zero. The horizontal red line represents a probability of 0.95.

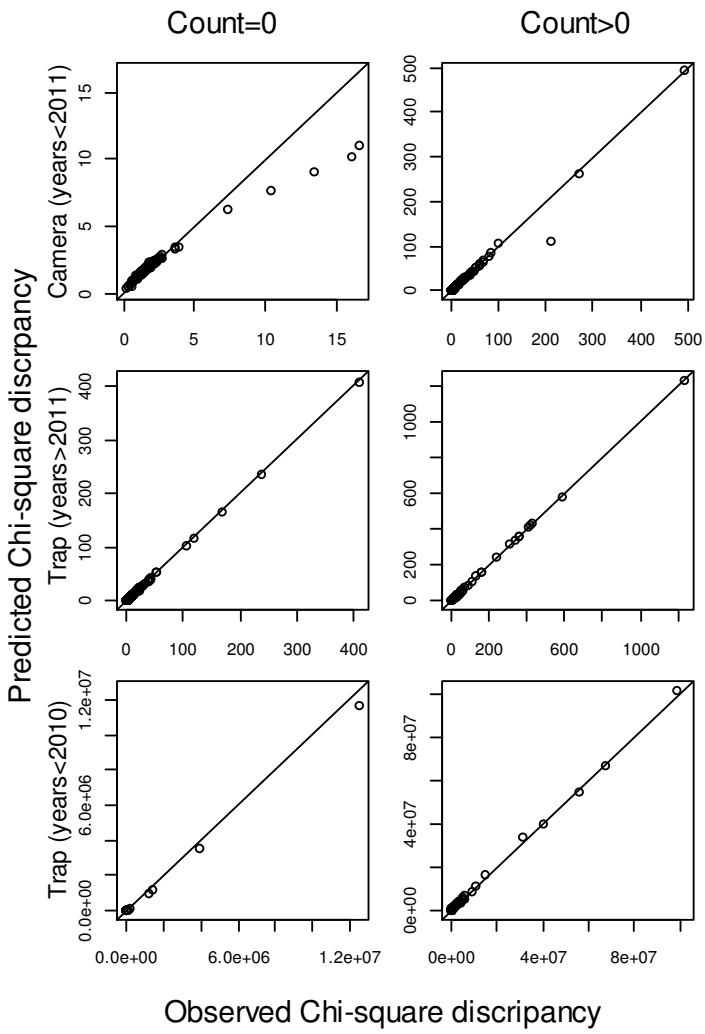

Figure D3. Residual plots of the observed and predicted Pearson residual for each model-fit reference site. The left column represents count data that are equal to zero, while the right column represents count data that are greater than zero.

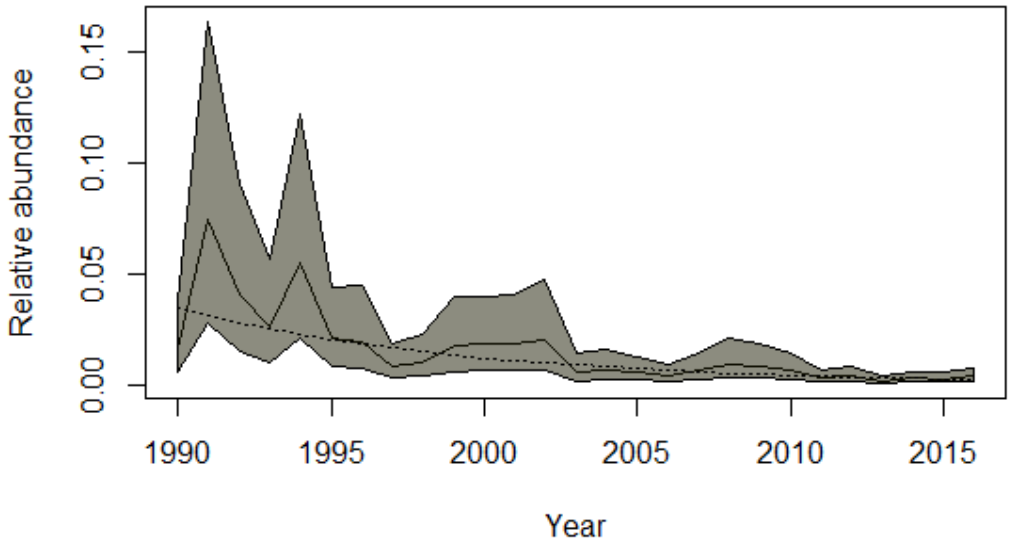

Figure D4. The predicted annual relative abundance of the vermilion snapper meta-population. The gray region represents 95% Bayesian credible intervals. The dotted line represents the estimated linear trend.

Appendix E. Model fit diagnostic plots (Log-N Poisson[abun &cam]).

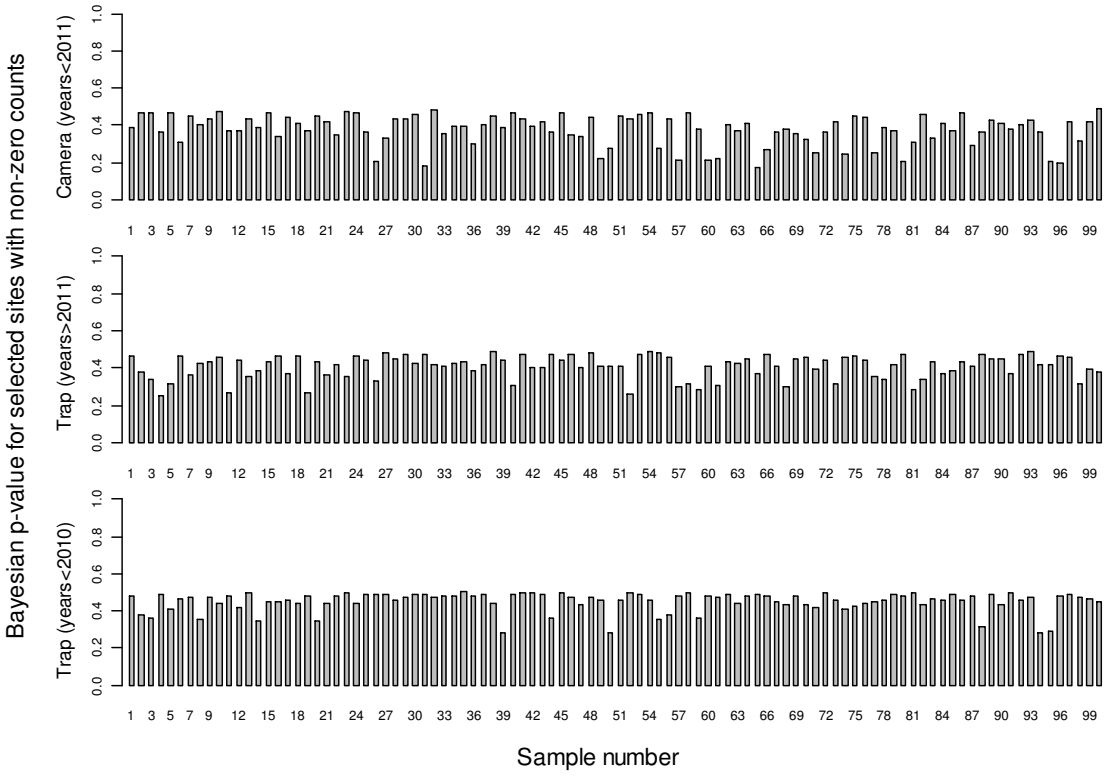

Figure E1. The Bayesian p-values for model-fit references sites with non-zero counts.

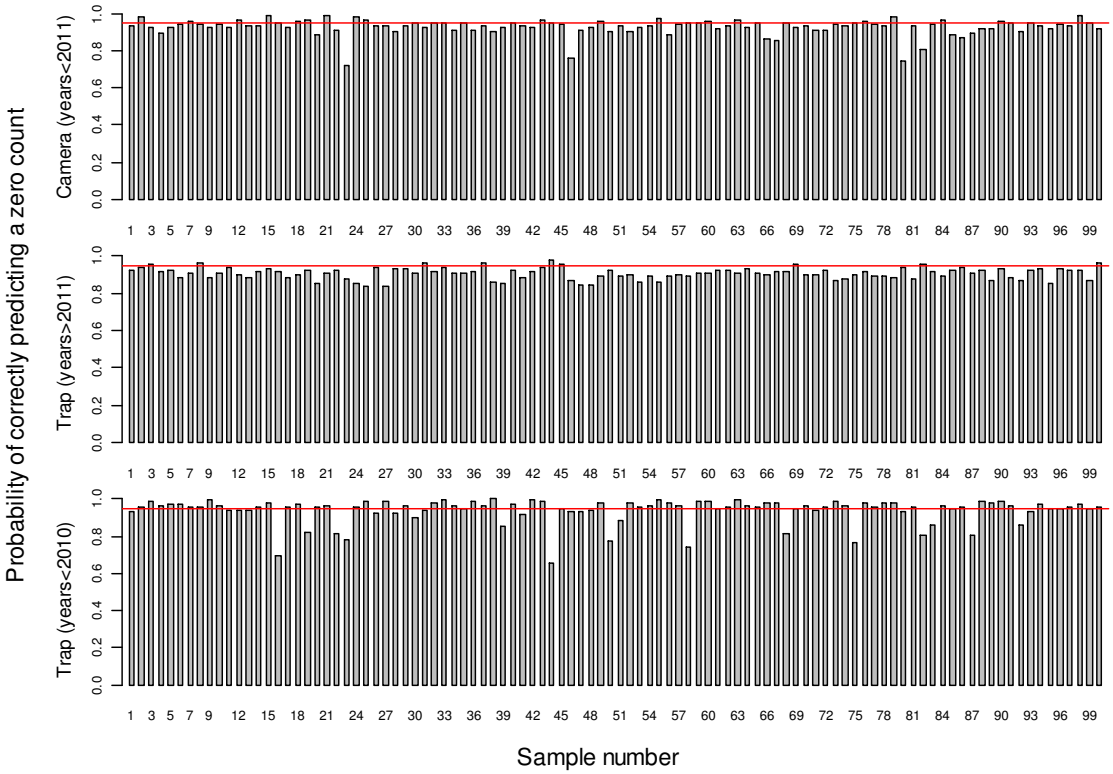

Figure E2. The model probability of correctly predicting a count equal to zero when the true count is zero. The horizontal red line represents a probability of 0.95

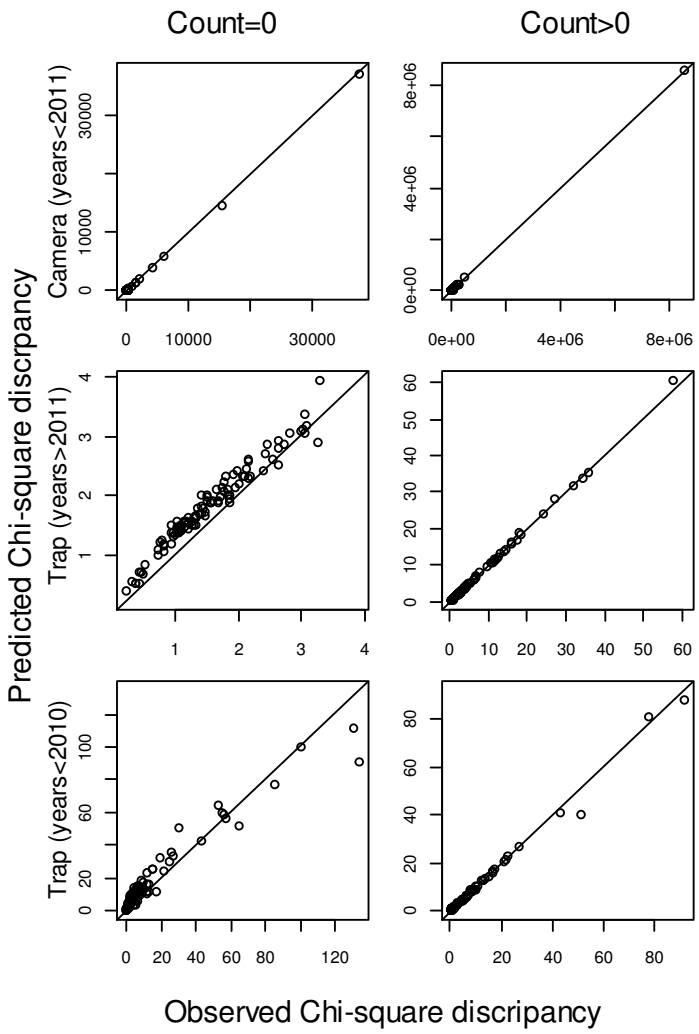

Figure E3. Residual plots of the observed and predicted Pearson residual value for each model-fit reference site. The left column represents count data that are equal to zero, while the right column represents count data that are greater than zero.

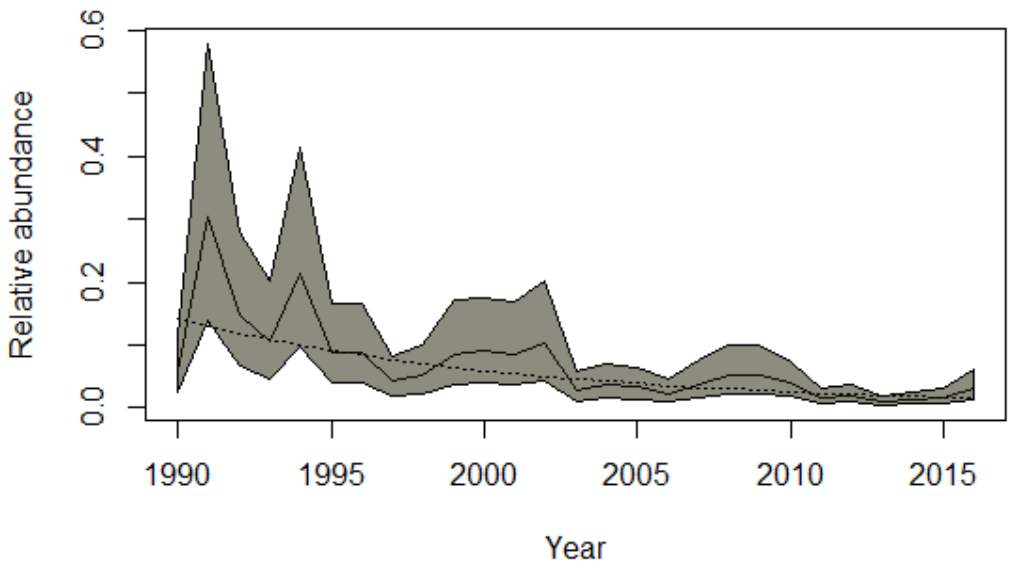

Figure E4. The predicted annual relative abundance of the vermilion snapper meta-population. The gray region represents 95% Bayesian credible intervals. The dotted line represents the estimated linear trend.

Appendix F. Model fit diagnostic plots (Log-N Poisson$^{cam\ \&\ trap}$).

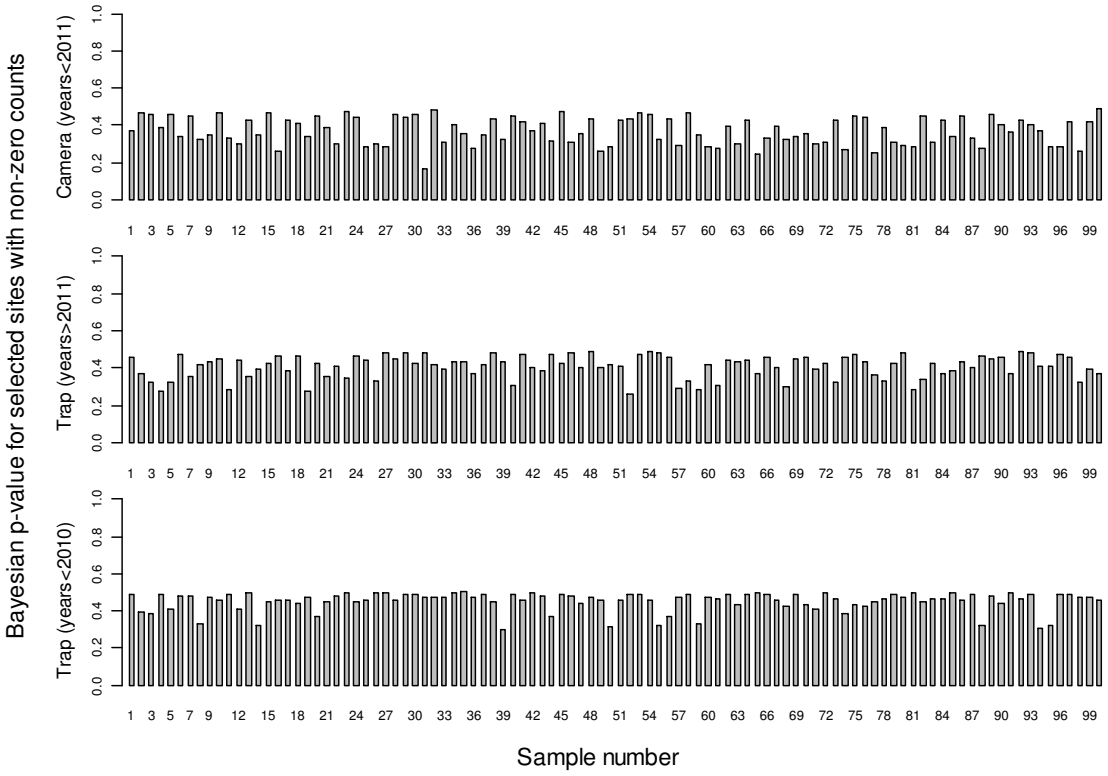

Figure F1. The Bayesian p-values for model-fit references sites with non-zero counts.

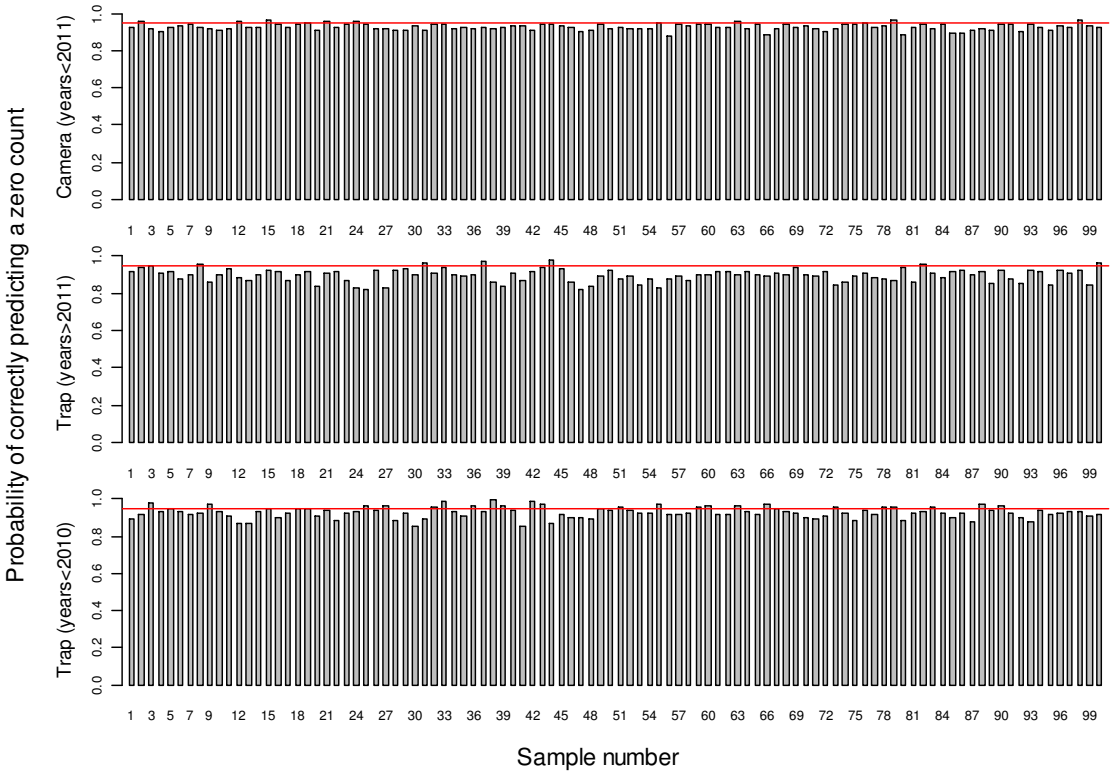

Figure F2. The model probability of correctly predicting a count equal to zero when the true count is zero. The horizontal red line represents a probability of 0.95.

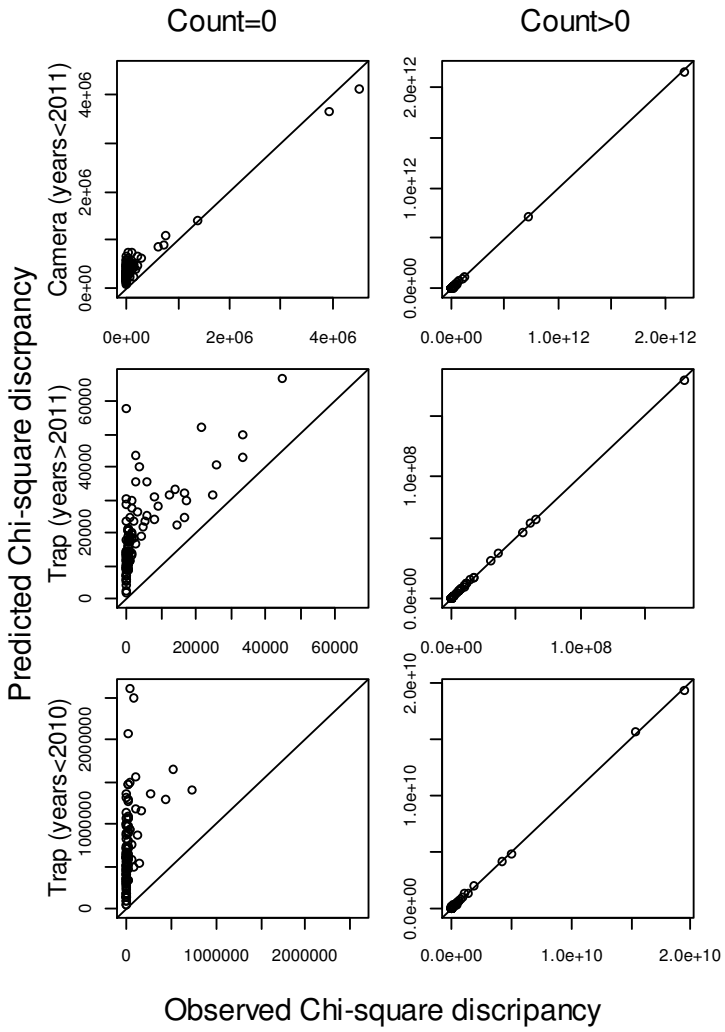

Figure F3. Residual plots of the observed and predicted Pearson residual value for each model-fit reference site. The left column represents count data that are equal to zero, while the right column represents count data that are greater than zero.

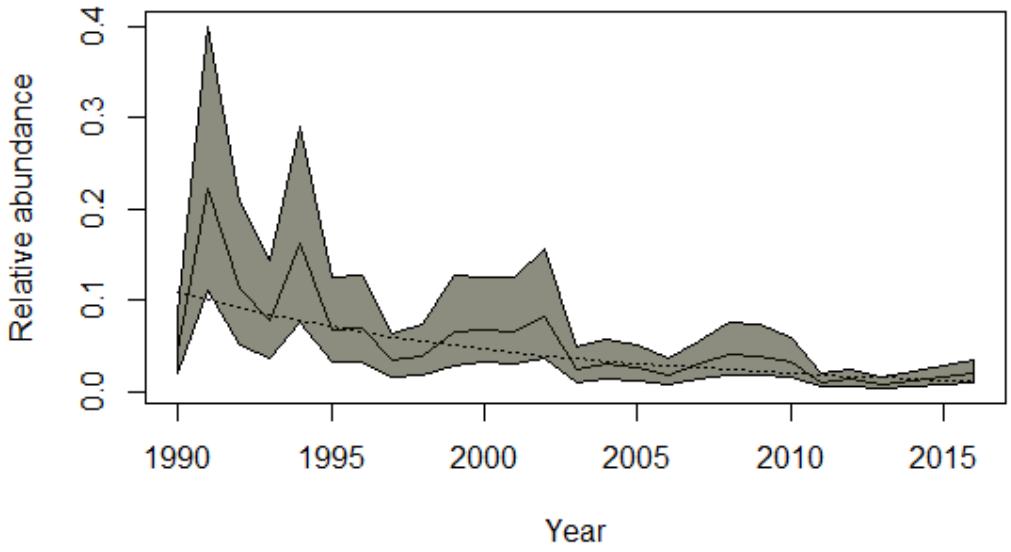

Figure F4. The predicted annual relative abundance of the vermilion snapper meta-population. The gray region represents 95% Bayesian credible intervals. The dotted line represents the estimated linear trend.

Appendix G. Model fit diagnostic plots (Log-N Poisson[abun]).

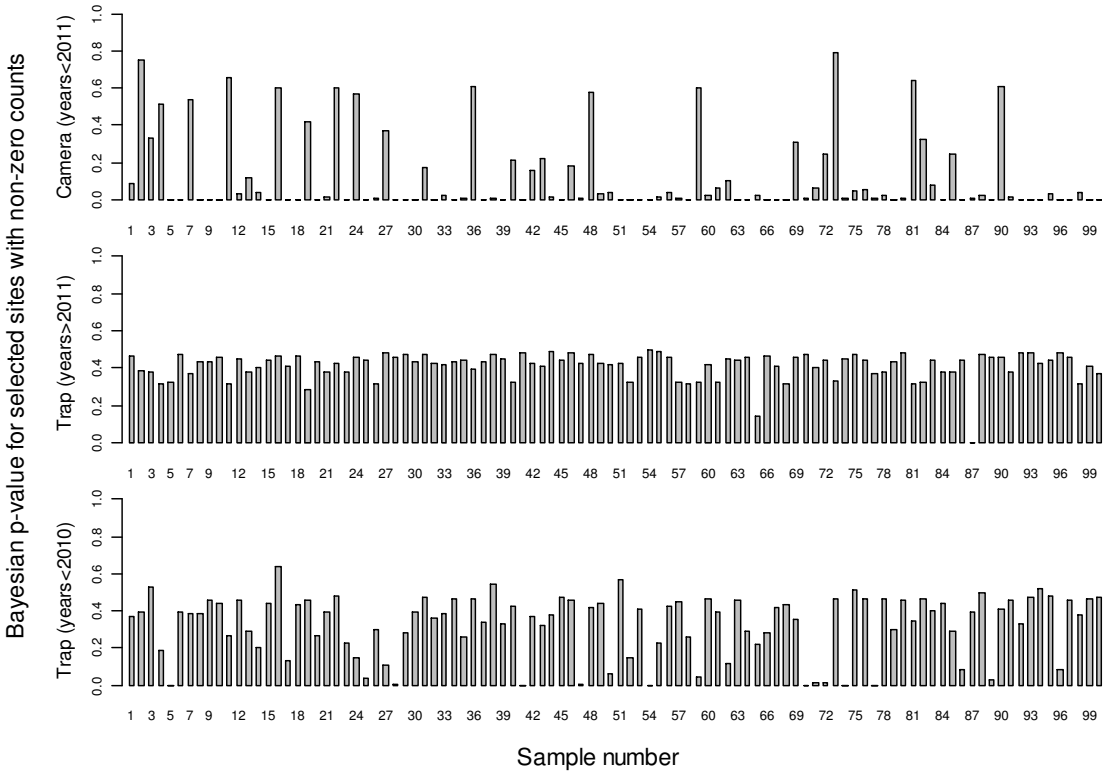

Figure G1. The Bayesian p-values for model-fit references sites with non-zero counts.

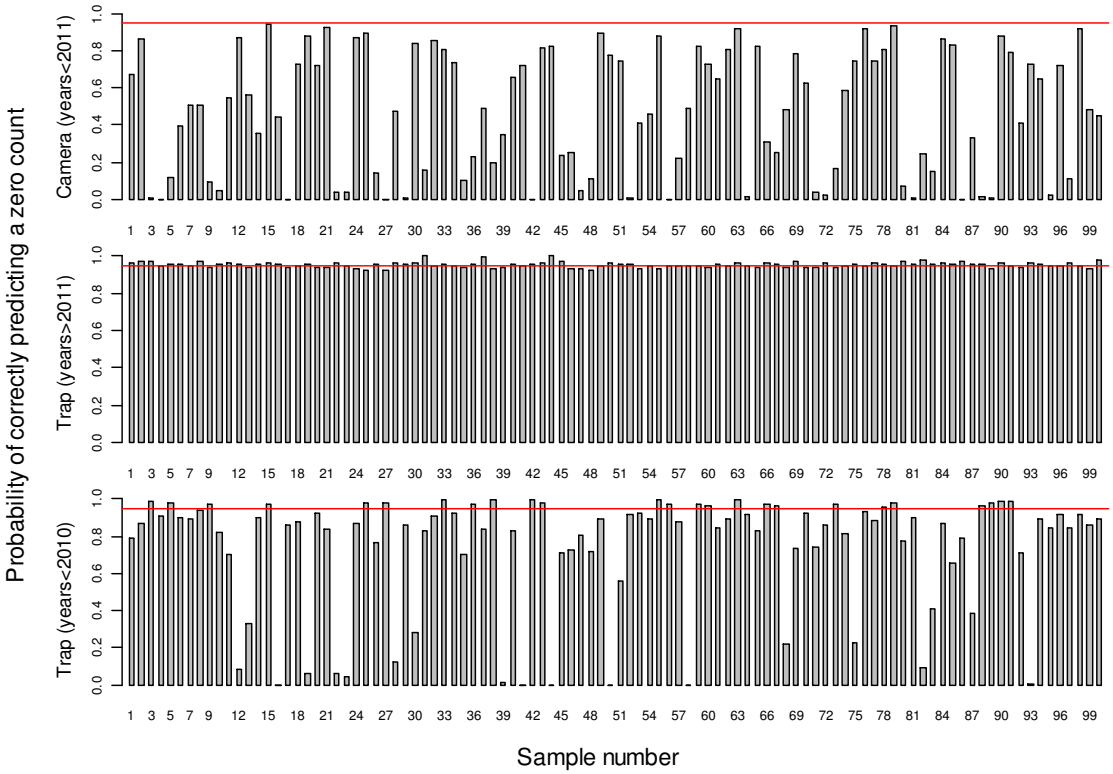

Figure G2. The model probability of correctly predicting a count equal to zero when the true count is zero. The horizontal red line represents a probability of 0.95.

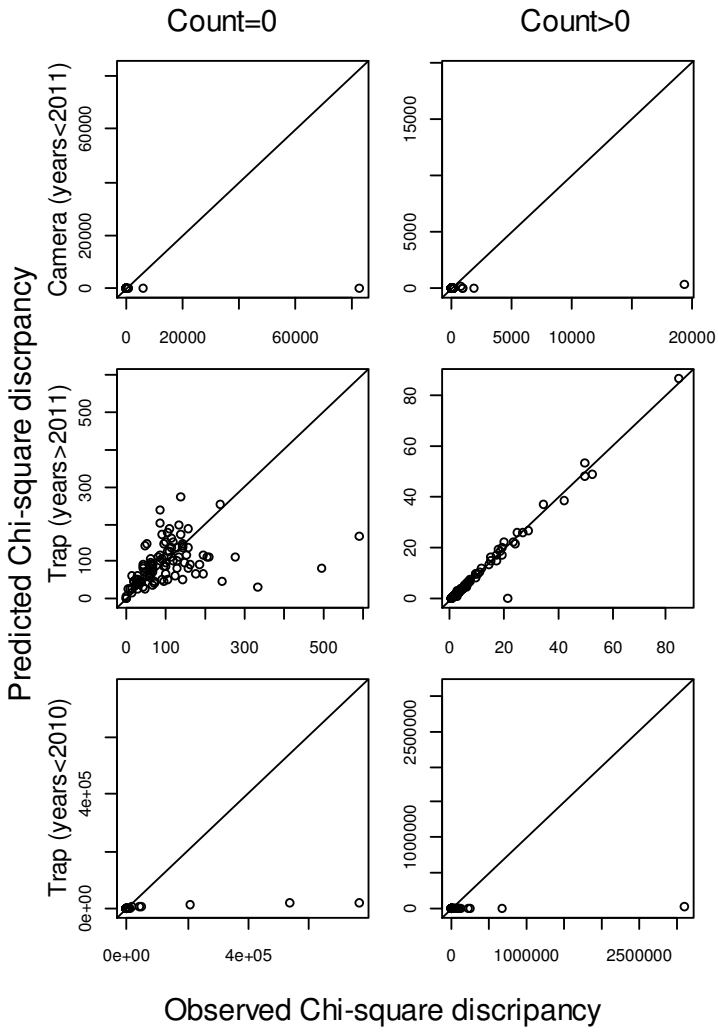

Figure G3. Residual plots of the observed and predicted Pearson residual for each model-fit reference site. The left column represents count data that are equal to zero, while the right column represents count data that are greater than zero.

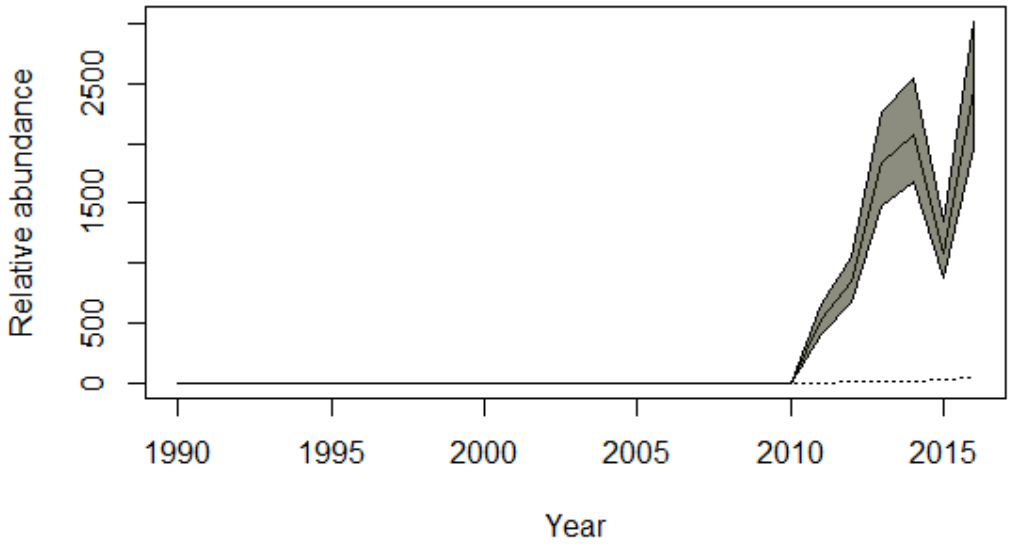

Figure G4. The predicted annual relative abundance of the vermilion snapper meta-population. The gray region represents 95% Bayesian credible intervals. The dotted line represents the estimated linear trend.

Appendix H. Model fit diagnostic plots (Log-N Poisson^{trap}).

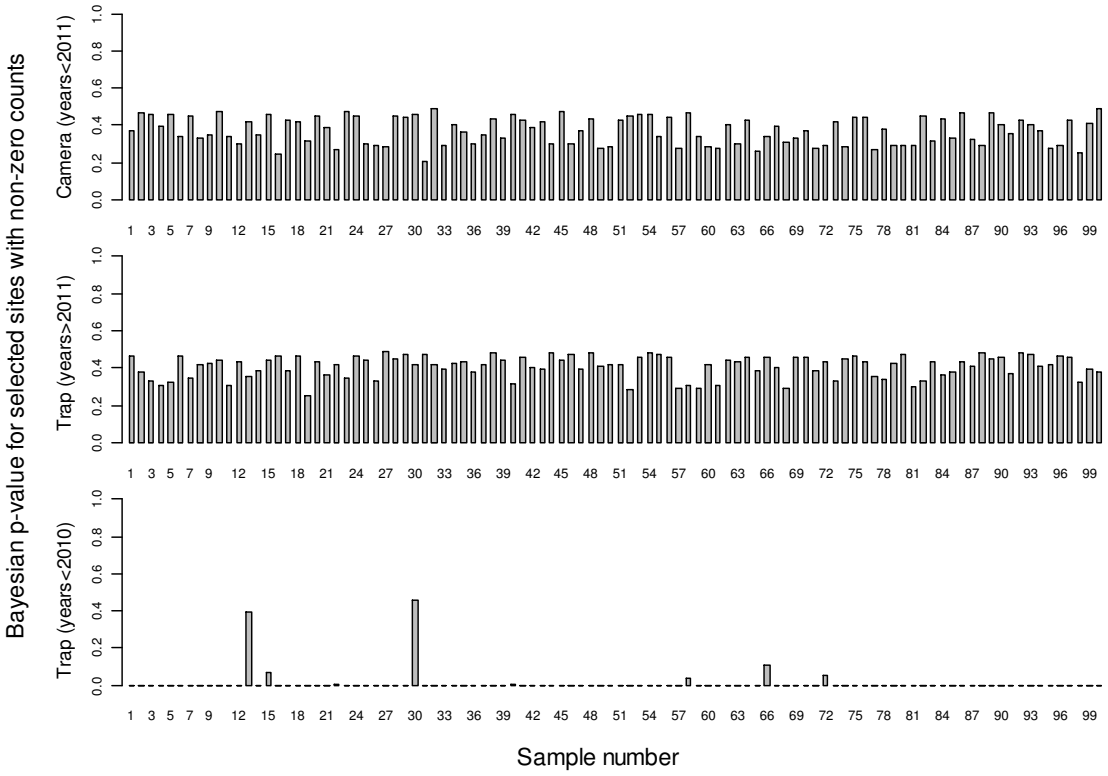

Figure H1. The Bayesian p-values for model-fit references sites with non-zero counts.

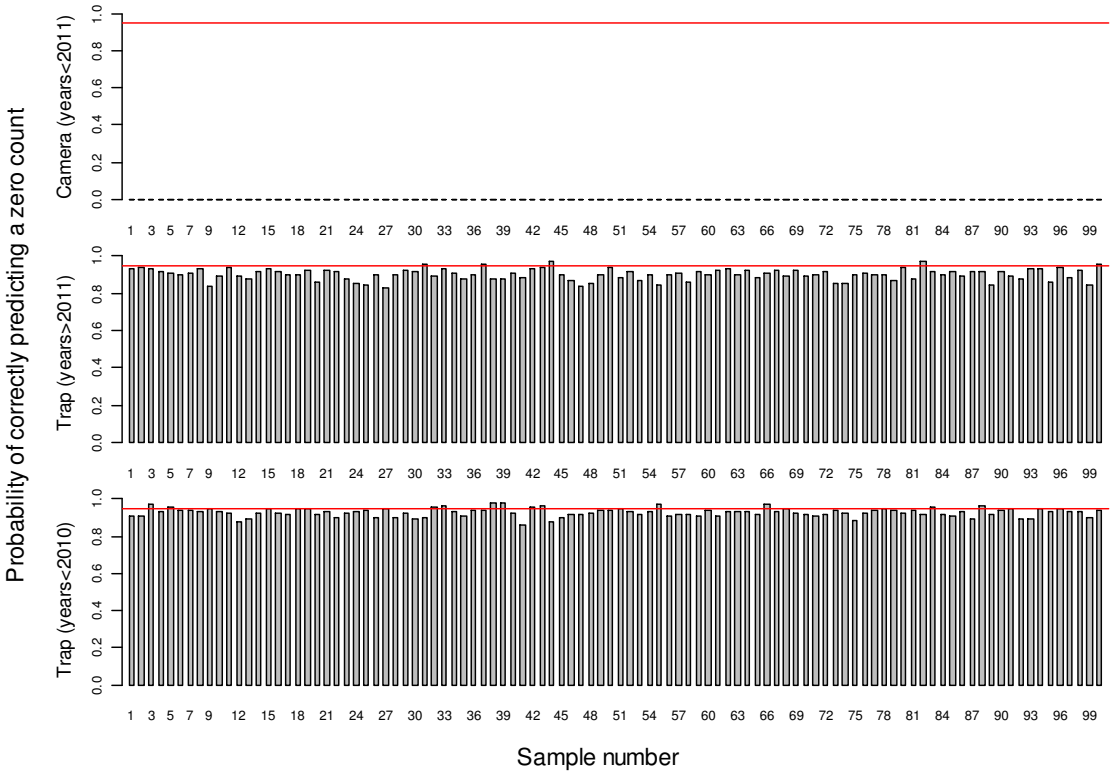

Figure H2. The model probability of correctly predicting a count equal to zero when the true count is zero. The horizontal red line represents a probability of 0.95.

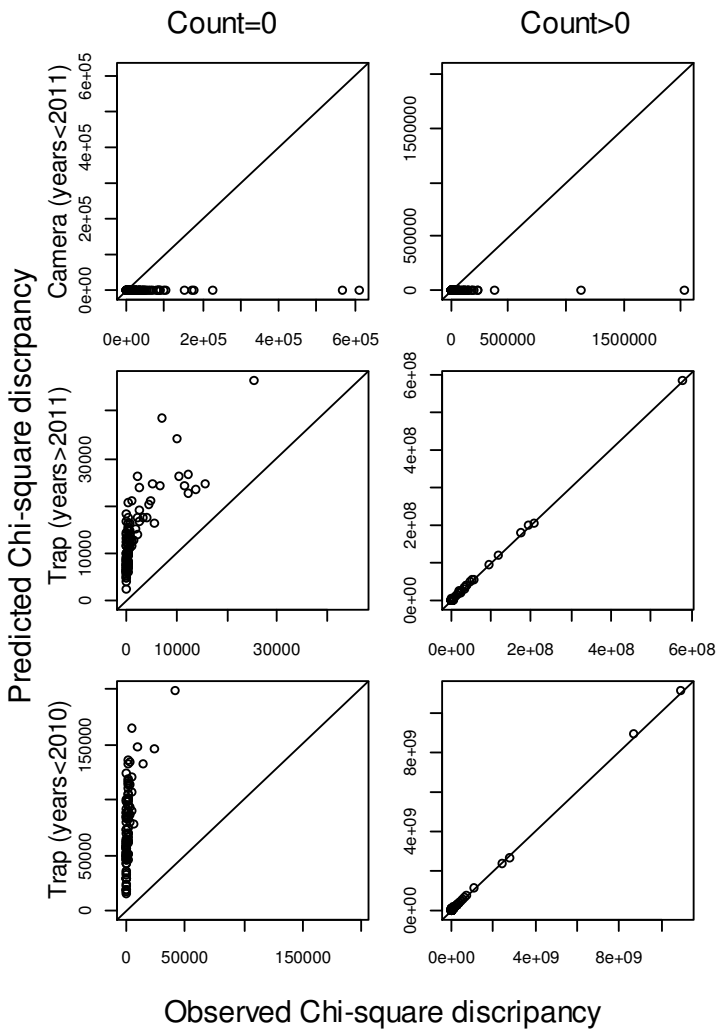

Figure H3. Residual plots of the observed and predicted Pearson residual for each model-fit reference site. The left column represents count data that are equal to zero, while the right column represents count data that are greater than zero.

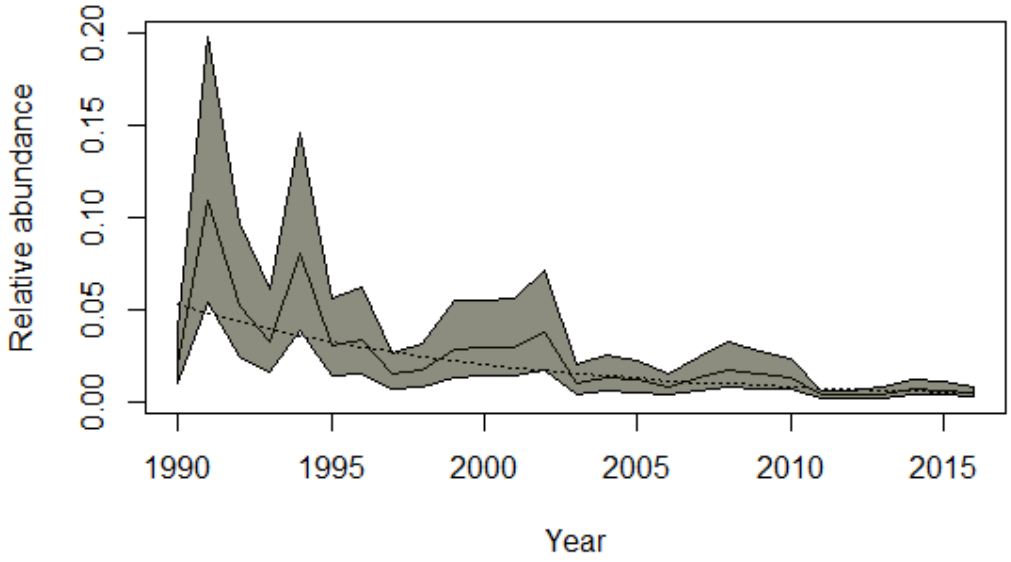

Figure H4. The predicted annual relative abundance of the vermilion snapper meta-population. The gray region represents 95% Bayesian credible intervals. The dotted line represents the estimated linear trend.

Appendix I. Model fit diagnostic plots (Log-N Poisson^{cam}).

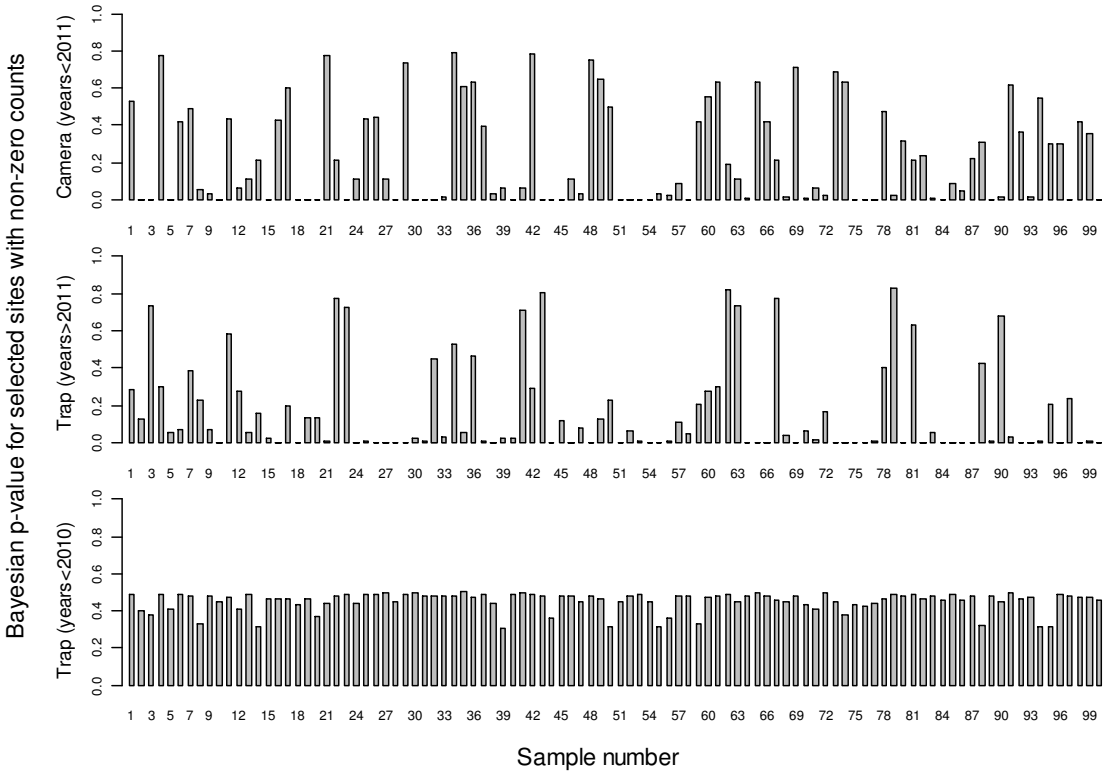

Figure I1. The Bayesian p-values for model-fit references sites with non-zero counts.

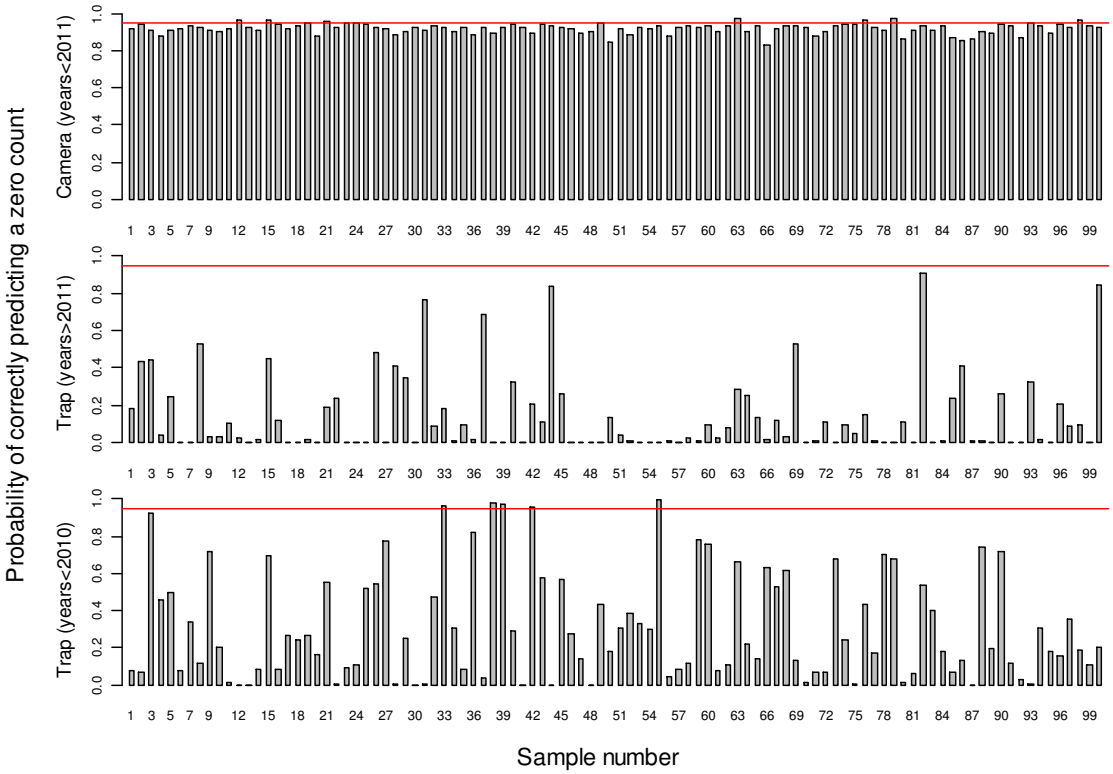

Figure I2. The model probability of correctly predicting a count equal to zero when the true count is zero. The horizontal red line represents a probability of 0.95.

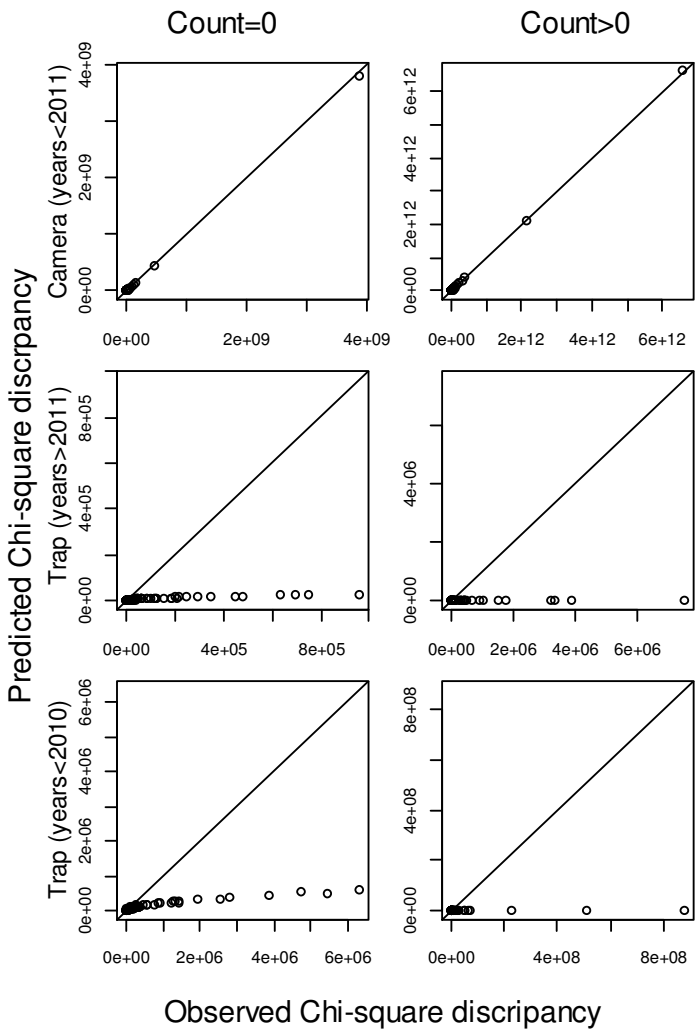

Figure I3. Residual plots of the observed and predicted Pearson residual for each model-fit reference site. The left column represents count data that are equal to zero, while the right column represents count data that are greater than zero.

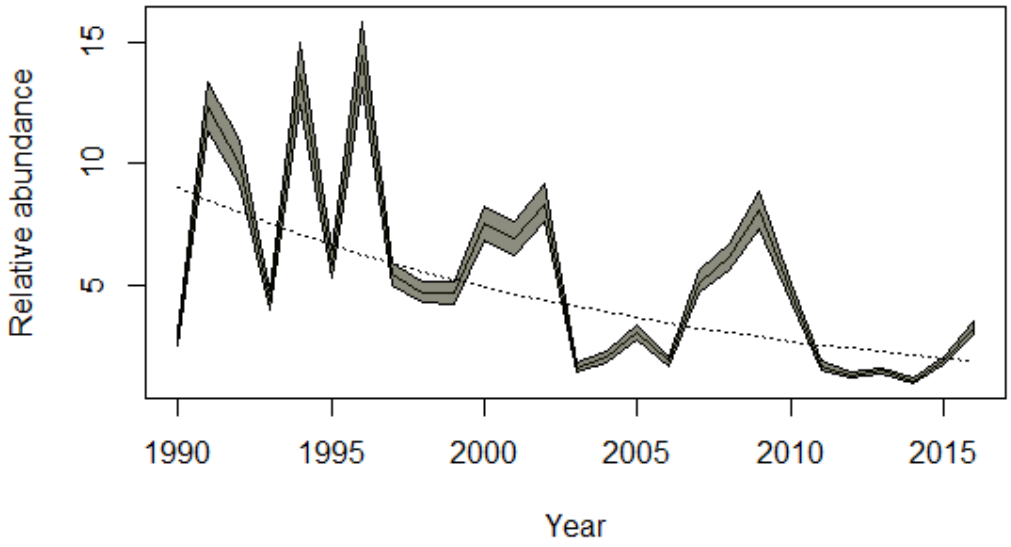

Figure I4. The predicted annual relative abundance of the vermilion snapper meta-population. The gray region represents 95% Bayesian credible intervals. The dotted line represents the estimated linear trend.

Appendix J. Model fit diagnostic plots (Log-N Poisson).

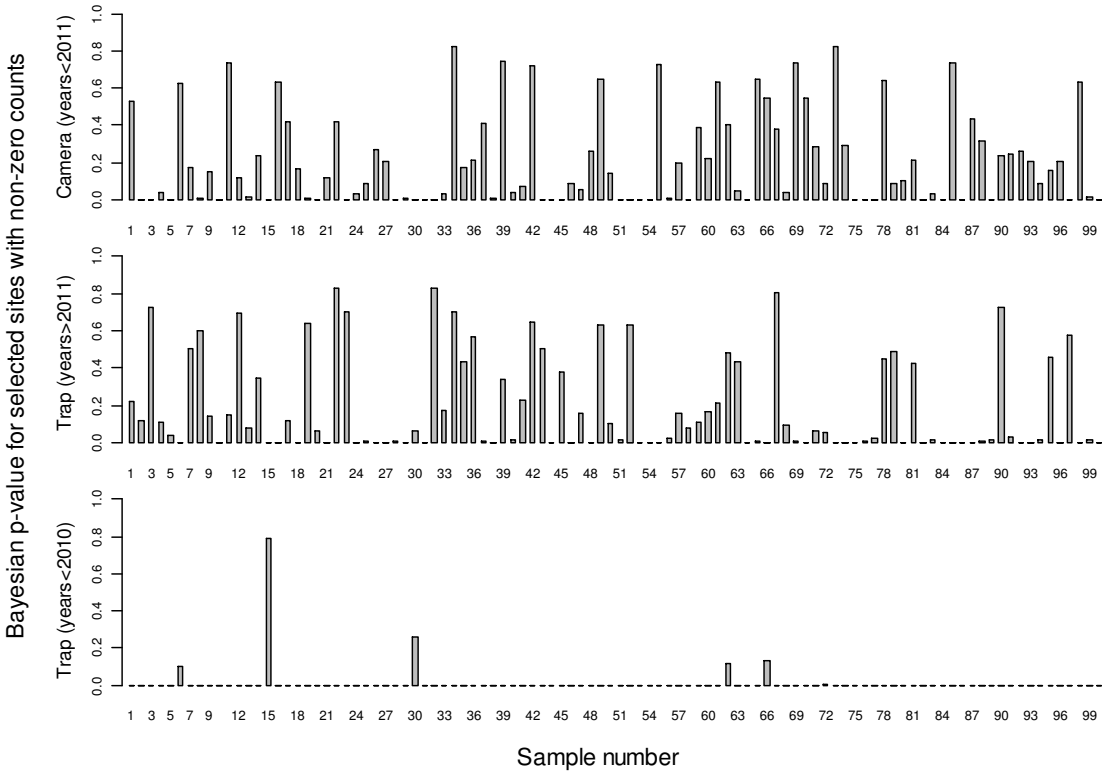

Figure J1. The Bayesian p-values for model-fit references sites with non-zero counts.

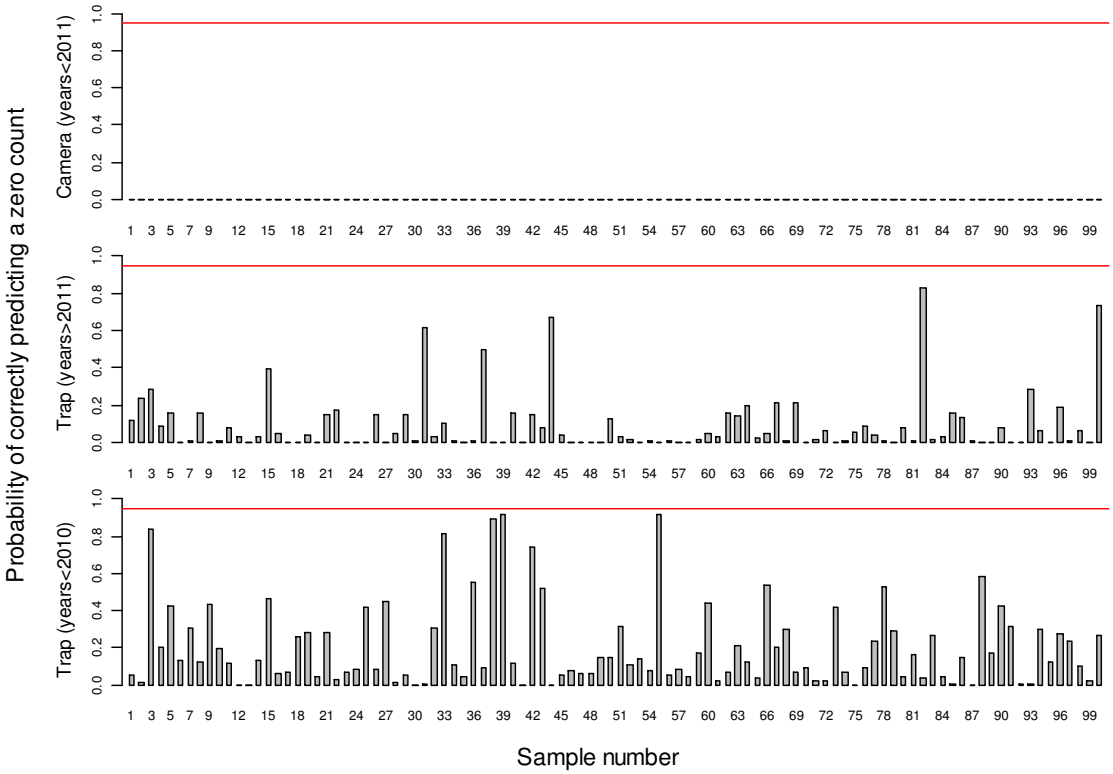

Figure J2. The model probability of correctly predicting a count equal to zero when the true count is zero. The horizontal red line represents a probability of 0.95.

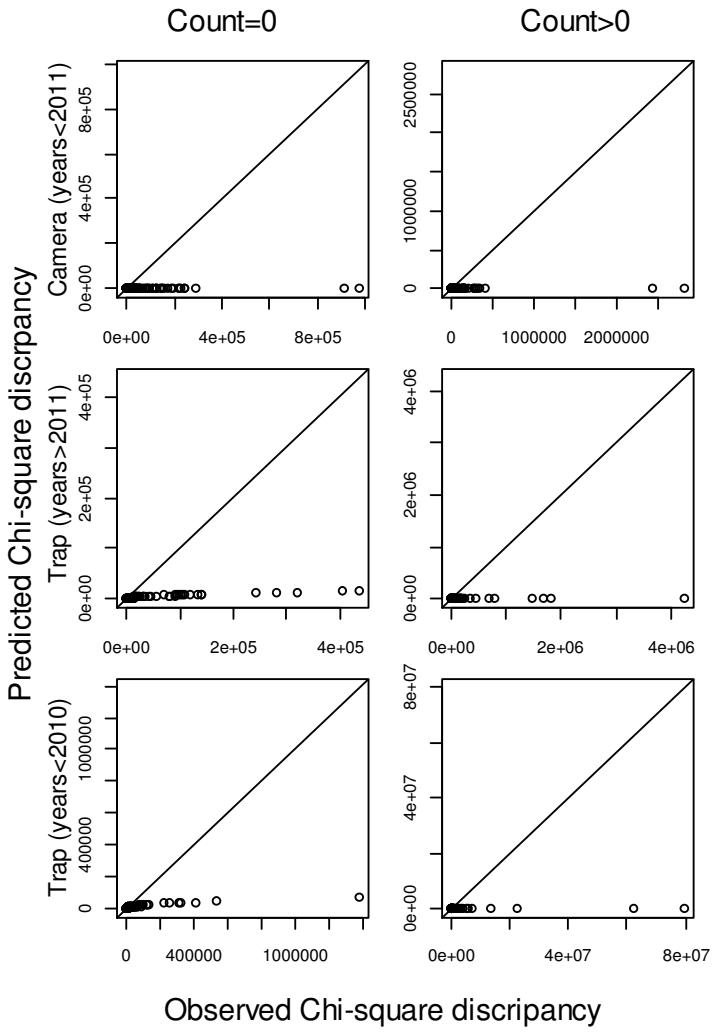

Figure J3. Residual plots of the observed and predicted Pearson residual for each model-fit reference site. The left column represents count data that are equal to zero, while the right column represents count data that are greater than zero.

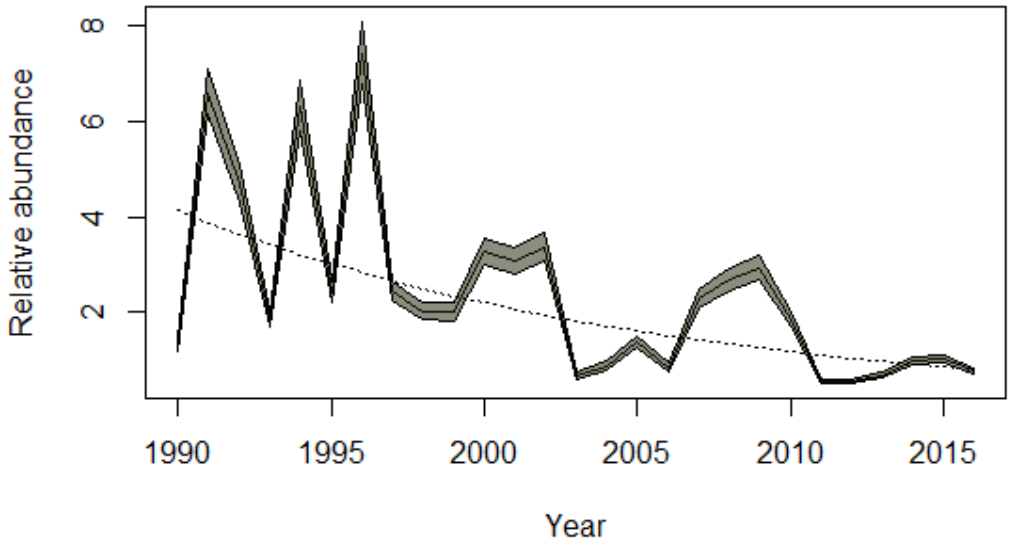

Figure J4. The predicted annual relative abundance of the vermilion snapper meta-population. The gray region represents 95% Bayesian credible intervals. The dotted line represents the estimated linear trend.

Appendix K. 95% Bayesian credible interval estimates for the three top models (Models 1-3 in Table 3).

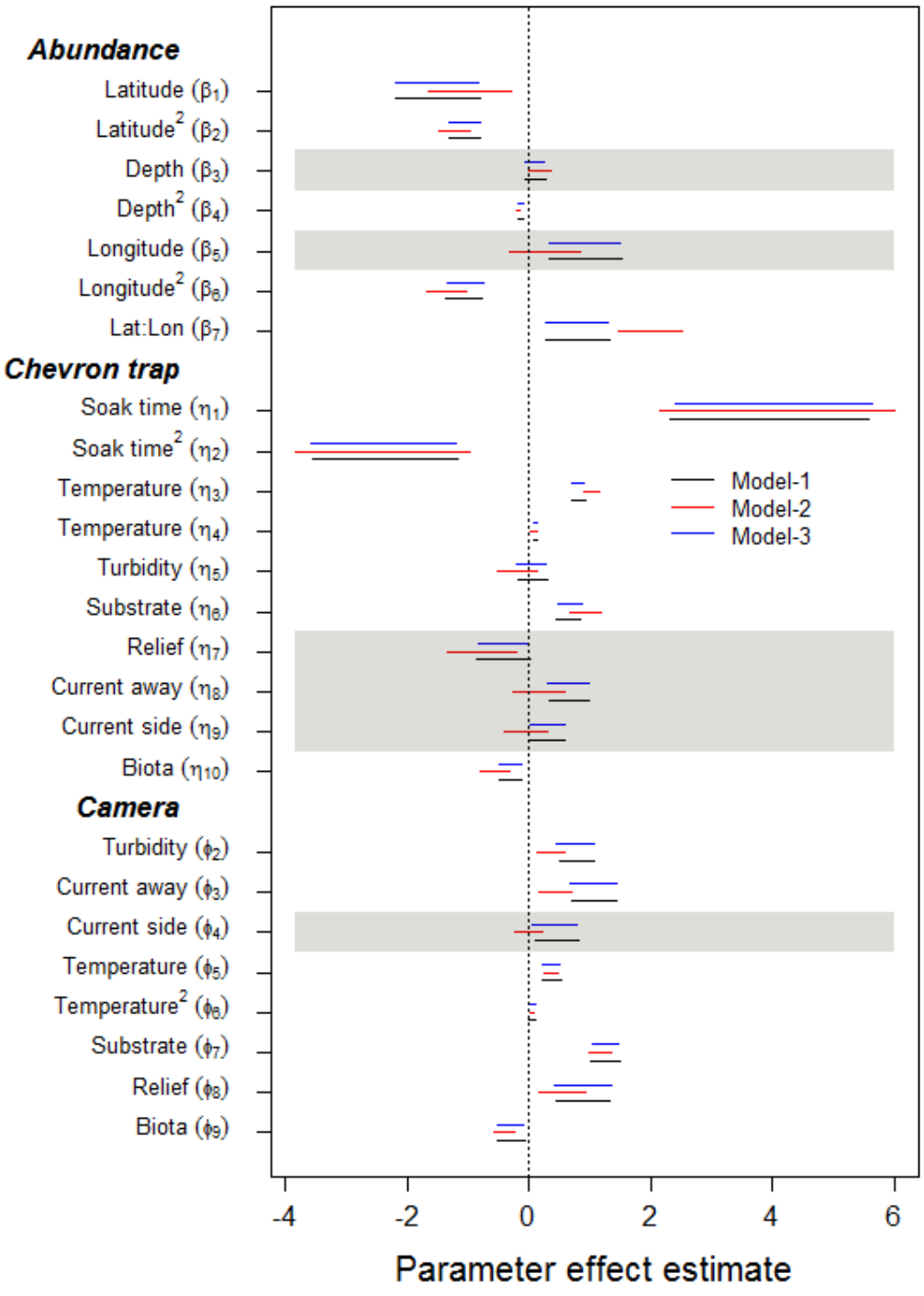

Figure K1. 95% Bayesian credible interval estimates for the three top models (Models 1-3 in Table 3). The shaded regions represent covariates whose statistical significance varies among models. Models 1, 2, and 3 are defined in Table 3 of the main document.